Atmos. Chem. Phys. Discuss., 13, 30521–30574, 2013
www.atmos-chem-phys-discuss.net/13/30521/2013/
doi:10.5194/acpd-13-30521-2013

Atmospheric Chemistry and Physics Discussions
Open Access

The isotopic composition of water vapour and precipitation in Ivittuut, Southern Greenland

J.-L. Bonne[1], V. Masson-Delmotte[1], O. Cattani[1], M. Delmotte[1], C. Risi[3], H. Sodemann[2], and H. C. Steen-Larsen[1]

[1]Laboratoire des Sciences du Climat et de l'Environnement, UMR8212, Gif sur Yvette, France
[2]Institute For Atmospheric and Climate Science, ETH Zurich, Zurich, Switzerland
[3]Laboratoire de Météorologie Dynamique, Paris, France

Received: 14 October 2013 – Accepted: 4 November 2013 – Published: 21 November 2013

Correspondence to: J.-L. Bonne (jean-louis.bonne@lsce.ipsl.fr)

Published by Copernicus Publications on behalf of the European Geosciences Union.

Abstract

Since September 2011, a Wavelength-Scanned Cavity Ringdown Spectroscopy analyzer has been remotely operated in Ivittuut, southern Greenland, providing the first continuous record of surface water vapour isotopic composition (δ^{18}O, δD) in South Greenland and the first record including the winter season in Greenland. This record depicts small summer diurnal variations. Measurements of precipitation isotopic composition suggest equilibrium between surface vapour and precipitation.

The vapour data show large synoptic and seasonal variations corresponding to shifts in moisture sources estimated using a quantitative moisture source diagnostic. The arrival of low pressure systems towards south Greenland leads to δ^{18}O enrichment (+5 ‰) and deuterium excess depletion (−15 ‰), coupled with moisture sources shifts.

Monthly δ^{18}O is minimum in November–December and maximum in June–July, with a seasonal amplitude of ∼ 10 ‰. The strong correlation between δ^{18}O and the logarithm of local surface humidity is consistent with Rayleigh distillation processes. The relationship with local surface air temperature is associated with a slope of ∼0.4 ‰ °C^{-1}. During the summer 2012 heat waves, the observations display a divergence between δ^{18}O and local climate variables, probably due to the isotopic depletion associated with long distance transport from subtropical moisture sources.

Monthly deuterium excess is minimum in May–June and maximum in November, with a seasonal amplitude of 20 ‰. It is anti-correlated with δ^{18}O, and correlated with local surface relative humidity (at the station) as well as surface relative humidity in a North Atlantic sector, south of Greenland and Iceland.

While synoptic and seasonal variations are well represented by the Atmospheric General Circulation Model LMDZiso for Ivittuut δ^{18}O, the model does not capture the magnitude of these variations for deuterium excess.

ACPD
13, 30521–30574, 2013

1 Introduction

Water stable isotopologues (H_2O, $H_2^{18}O$ and HDO) in atmospheric waters are widely used as tracers of the hydrological cycle (Jouzel, 2003). In Greenland ice cores, water stable isotopes have been used to quantify past changes in climate and in the water cycle. Because this motivates a better understanding of the processes at play from present-day studies, we briefly summarize the key findings and questions arising from these ice core studies.

A brief description of water isotopes basics is given hereafter. The isotopic composition of water is expressed in ‰ unit, using δ notations, defined as a variation of the sample isotopic ratio R compared to a standard isotopic ratio R_{VSMOW}:

$$\delta = 1000 \times (R/R_{\mathrm{VSMOW}} - 1) \quad (1)$$

In this work, we focus on $\delta^{18}O$ and δD isotopic compositions (corresponding to $H_2^{18}O$ and HDO isotopologues) of water vapour and precipitation, based on in situ continuous observations. Hereafter, precipitation and vapour observations are respectively noted with the suffixes p and v.

Since water stable isotopologues have different saturation vapour pressure and diffusivity in the air, fractionation processes occur during phase changes (such as evaporation or condensation). They produce strong temporal and spatial variations of atmospheric water vapour and precipitation isotopic composition. These variations are driven by continuous removal of heavier isotopes during poleward transport, sometimes called atmospheric distillation, and are affected by changes in moisture sources and transport histories. As changes in temperature strongly control this distillation and the isotopic composition of precipitation at mid and high latitudes, this forms the basis for past temperature reconstructions using records of precipitation isotopic composition in archives such as ice cores (Jouzel, 2003). In addition to equilibrium fractionation, kinetic processes take place for instance during evaporation or condensation on ice crystals. The second order parameter deuterium-excess (hereafter noted d,

ACPD
13, 30521–30574, 2013

$d = \delta D - 8 \times \delta^{18}O$) has been introduced to identify deviations from the mean relationship between $\delta^{18}O$ and δD in meteoric waters (with a mean slope of 8 resulting from equilibrium fractionation) and highlight kinetic effects (Dansgaard, 1964; Craig and Gordon, 1965; Merlivat and Jouzel, 1979).

Greenland ice core records now cover 140 000 yr (Dahl-Jensen et al., 2013). High resolution records have documented the seasonal cycle of surface snow isotopic composition (Johnsen, 1977), and seasonal changes during the past millennia (Vinther et al., 2010). Initially, the quantitative interpretation of Greenland ice core water stable isotope records in terms of temperature was based on an isotope-temperature relationship following modern spatial surface snow and precipitation data, and surface air or firn temperatures (Dansgaard, 1964; Sjolte et al., 2011). The comparison of past temperatures inferred from borehole temperature profiles and from gas fractionation (Severinghaus and Brook, 1999; Dahl-Jensen et al., 1998; Cuffey et al., 1992; Vinther et al., 2010; Masson-Delmotte et al., 2011) has demonstrated that the isotope-temperature relationship varies through time, possibly due to changes in precipitation seasonality (Krinner et al., 1997; Krinner and Werner, 2003) and intermittency (Persson et al., 2011), and in moisture origin. Statistical and backtrajectory analysis have depicted a strong imprint of the North Atlantic Oscillation (NAO), associated with large shifts of the mean moisture sources, in winter and annual ice core isotopic signals, consistent with its imprint in instrumental temperature records (Vinther et al., 2010; Casado et al., 2012; Sodemann et al., 2008b, a). Rapid strong shifts in d have been documented during abrupt events (Steffensen et al., 2008; Thomas et al., 2009), together with significant changes at the orbital scale, possibly related to major changes in moisture sources (Masson-Delmotte et al., 2005; Jouzel et al., 2007). The combination of different ice core records has recently allowed to investigate the regional patterns of past changes in precipitation water stable isotopes and climate (Steen-Larsen et al., 2011; Guillevic et al., 2012). All these studies point out that the quantitative understanding of Greenland ice core records requires improved comprehension of the different processes controlling Greenland surface snow isotopic composition. This calls for

ACPD
13, 30521–30574, 2013

a continuous monitoring of water vapour, precipitation and surface snow isotopic composition, in order to decipher, at the atmospheric process scale, the drivers of transport, deposition and post-deposition effects.

Under the auspices of the GNIP/IAEA (Global Network of Isotopes in Precipitation/International Atomic Energy Agency), Greenland coastal precipitation has been sampled at different locations and analysed for water stable isotope composition, at the monthly scale, during specific time intervals (Rozanski et al., 1993; Sjolte et al., 2011), limiting the analyses to seasonal timescales. The isotopic composition of Greenland water vapour has remained for long undocumented, due to the difficulty of trapping water vapour without fractionation and the manpower requested for manual cold trap sampling (Jacob and Sonntag, 1991). A recent monitoring effort has been implemented at the NEEM Greenland ice core drilling site. During summer, precipitation, surface water vapour and surface snow were sampled for isotopic measurements (Steen-Larsen et al., 2011, 2013a, b), in order to better understand the post-deposition processes affecting the ice core signals. The data have shown that the surface water vapour is in isotopic equilibrium with the snowfall and the surface snow. A water vapour cold trap sampling campaign has also been conducted above the Arctic Ocean onboard a research vessel (Kurita, 2011). Combined with Siberian precipitation data, the data suggest a specific fingerprint of moisture formed at the sea-ice margin, in autumn, where dry air can produce a large kinetic fractionation and produce high d values. So far however, no study has been dedicated to the water vapour at coastal and southern Greenland locations and during winter season over all Greenland, which should allow to investigate the isotopic fingerprints of North Atlantic moisture sources.

In recent years, new types of infra-red laser spectrometers have been developed, allowing high frequency in situ measurements of water vapour isotopic composition. If an appropriate measurement and calibration protocol is applied (Tremoy et al., 2011; Aemisegger et al., 2012; Steen-Larsen et al., 2013a), these instruments reach a precision close to classical instruments based on Isotope-Ratio Mass Spectrometry. In the Arctic region, data have been reported for Siberia, showing large magnitude syn-

ACPD
13, 30521–30574, 2013

optic events (Gribanov et al., 2013), and in summer at NEEM (Steen-Larsen et al., 2013a). These NEEM data have evidenced a diurnal variability, attributed to snow–air water vapour interactions, and synoptic events, with a potential signature of Arctic air masses through high *d* events.

Our study is focused on the atmospheric monitoring station of Ivittuut, southern Greenland, situated close to Grønnedal where precipitation isotopic composition were measured by GNIP/IAEA in the 1960s–1970s (see Supplement Sect. A). This site is situated almost at sea level, and is therefore complementary of the monitoring conducted during several summer field seasons at the NEEM site, at an elevation of 2500 m a.s.l. (Steen-Larsen et al., 2013a). In September 2011, we have implemented a water vapour stable isotope analyzer in this station. Our observation period covers events of strong heat waves in summer 2012, associated with strong advection of heat and humidity from further south (Fettweis et al., 2013; Bennartz et al., 2013; Nghiem et al., 2012; Neff et al., 2013). The drivers of our isotopic signals are investigated using a Lagrangian moisture source identification (Sodemann et al., 2008b) and the LMDZiso nudged isotope-enabled Atmospheric General Circulation Model (AGCM) model (Risi et al., 2010a). AGCM simulations allow to explore the spatial representativeness of station data, but also to assess if the model correctly resolves the meteorological drivers of the local water vapour isotopic composition.

This manuscript is organized in five sections. Section 2 describes material and methods. Section 3 is dedicated to the description of the water vapour and precipitation isotopic data and their relationship with local climate and the influence of changes in moisture transport. Section 4 confronts Ivittuut observations to LMDZiso simulations. Conclusions and perspectives are given in Sect. 5.

2 Methods and data

In this section, we focus on the methods used for the acquisition of the different datasets used in the next sections. Section 2.1 describes the station where meteoro-

ACPD
13, 30521–30574, 2013

logical observations (presented in Sect. 2.2) and water vapour isotopic composition observations are performed. Section 2.3 describes the monitoring of precipitation isotopic composition and the associated calculation of water vapour isotopic composition. Section 2.4 is dedicated to the water vapour isotopic composition monitoring and presents the instrumental protocol and the data treatment chain. In Sect. 2.5 are summarized the instrument set-up difficulties and improvements, and the data quality. Sections 2.7 and 2.8 respectively present the large scale atmospheric models used for data interpretation: FLEXPART Lagrangian dispersion model, and LMDZiso Atmospheric General Circulation Model with water isotopes.

2.1 Sampling site

The atmospheric monitoring station of Ivittuut, southern Greenland (61.21° N, 48.17° W, altitude 30 m a.s.l.), depicted in Fig. 1, was established in Autumn 2007 for the monitoring of CO_2 and O_2/N_2 atmospheric mixing ratios, giving access to Atmospheric Potential Oxygen (Stephens et al., 1998). The site was chosen in order to study the role of the North Atlantic Ocean as a carbon sink, as part of the EU CarboOcean project. Thanks to partnerships established with local authorities (Kommuneqarfik Sermersooq) and the Danish navy (Greenland Kommando, GLK), the atmospheric observatory has been installed with logistical support from both sides.

This Greenlandic coastal site is located 100 m from the Arsuk Fjord, at approximately 5 km east of the open ocean and 10 km west of the ice sheet. Arctic vegetation, mainly bushes and grasslands, is present in the valley, surrounded by mountains. A few buildings from an abandonned cryolite mine have been renovated in Ivittuut, located 5 km from the Grønnedal village and Danish Navy military base (Fig. 1). A meteorological station was set up in Autumn 2007, measuring temperature, pressure, relative humidity, wind speed and direction. In September 2011, new instruments have been installed in order to monitor the CH_4 mixing ratio as well as water vapour isotopic composition (see next sections). All instruments are located in a heated building. Electricity is provided by the Ivittuut power station, situated about 100 m from the station. Basic maintenance is

ACPD
13, 30521–30574, 2013

operated by technicians from the Danish Navy. Heavy maintenance is conducted once a year by LSCE (Laboratoire des Sciences du Climat et de l'Environnement, Saclay, France).

Measurements from the atmospheric monitoring instruments are automatically transferred to LSCE. Online access allows daily monitoring and control of the instruments.

2.2 Meteorological data

High frequency (around 1 Hz) meteorological measurements have been obtained at Ivittuut station since September 2007. Temperature and relative humidity are measured by a Vaisala humidity and temperature Probe HMP155 (situated 1.8 m above ground), wind direction and speed by a Young sensor (model 05603B) (situated on the roof top, about 3.5 m above ground), and pressure by a Druck RPT 410 sensor (1.8 m above ground). A failure of the sensor acquisition card led to several gaps in the acquisition of the data during the observation period (see Sect. 3).

Complementary historical meteorological information is available from the measurements at Grønnedal with the framework of GNIP/IAEA, from 1961 to 1974 (available at http://nucleus.iaea.org/CIR/CIR/GNIPIHIS.html, 2013).

2.3 Precipitation water stable isotope data and equilibrium vapour isotopic calculations

Monthly historical isotope observations of precipitation in Grønnedal are available through the GNIP/IAEA network from 1961 to 1974 included.

In September 2011, two rain gauges have been installed, one in Ivittuut and one in Grønnedal. Water is sampled manually at an approximate weekly frequency for Grønnedal rain gauge and an approximate bi-weekly frequency for Ivittuut rain gauge. Water samples are stored in glass bottles closed with plastic caps and packed in cellophane film after sampling. They are then shipped and analysed at LSCE using mass spectrometer or Picarro liquid water isotope analyser, with accuracies of 0.7‰ for δD_p

ACPD
13, 30521–30574, 2013

and 0.025‰ for $\delta^{18}O_p$ (resulting in 0.9‰ for d_p). The type of precipitation (liquid or snow) is recorded, depending of the water phase in the collector at the time of sampling, as well as the precipitation amount. Both rain gauges underwent damages caused by winter storms, leading to gaps in the precipitation data. The most complete dataset is the one from Grønnedal, ranging from October 2011 to November 2012, with a gap from June to August 2012.

After discarding samples affected by storage effects (frozen in the collector or affected by evaporation), we obtained 6 validated samples in Ivittuut from 15 September 2012 to 1 March 2012 and 39 validated samples in Grønnedal from 16 September 2011 to 5 November 2012.

Water vapour isotopic composition in equilibrium with the precipitation have been calculated using the fractionation coefficient at equilibrium α for $\delta^{18}O$ or δD, from Majoube (1971a, b); Merlivat and Nief (1967). For all precipitation sample isotopic ratio R_P, we obtain vapour isotopic ratio $R_V = R_P/\alpha$. Depending on the physical phase of the precipitation found in the collector, we used fractionation coefficients between liquid and vapour phases (for liquid samples), or between solid and vapour phases (for snow samples). Because the exact time and date of the precipitation event is not known, α coefficients are calculated in first approximation considering the average surface temperature observed at the station during the complete period between two precipitation samplings.

2.4 Water vapour isotope monitoring

A Picarro brand model L2120-i Wavelength-Scanned Cavity Ringdown Spectroscopy (WS-CRDS) analyzer, hereafter Picarro, was installed in September 2011 at Ivittuut station, in the basement of the building to ensure a better temperature stability in the room. The experimental design and data treatment procedure are similar to those described in Gribanov et al. (2013). Ambient air is sampled through a 10 m long and 3/8 inch diameter O'Brien analytical True Tube EPS (inox 316L chromium electropolished),

ACPD
13, 30521–30574, 2013

a material chosen to limit wall effects between the inner tube and the water vapor in the air sample. Air is sampled about 5 m a.g.l. The sampling line is temperature autoregulated (Wheatstone bridge) and protected against rain, snow and insects by a hard cover and a net. An automatic calibration system using the Picarro brand Standard Delivery Module (SDM) is used to measure the isotopic composition of vaporized water standards, calibrated on the VSMOW scale by accurate laboratory mass spectrometer measurements. Two water standards, EPB and GREEN (Table 1), are injected by SDM in the Picarro brand Vaporizer and vaporized at 140 °C, then mixed with dry air (room air dessicated with DRIERITE changed every one or two months depending of the ambient air humidity) and measured by the analyzer. Adjusting the liquid water and/or dry air flow levels allows to measure the water standards at different humidity levels. Several adjustments during our observation period, summarized in Table 2, led to more stable calibrations.

The influence of the humidity level on laser-spectroscopic stable isotope measurements as been identified in several recent calibration studies, and appears dependent on the instrument and the calibration system (Aemisegger et al., 2012; Tremoy et al., 2011; Steen-Larsen et al., 2013a). To assess the humidity-isotope response function of our instrument, both water standards were measured at different humidity levels from 1000 to 17 000 ppmv (Fig. 2). This test was performed on field in October 2012 and is assumed to remain stable. The response functions were fitted for each isotope and each standard, with the best fit obtained using the following equations giving δX (either δ^{18}O or δD) as a function of humidity H_2O_{ppmv}:

$$\delta X = a + \frac{b}{H_2O_{ppmv}} + \frac{c}{(H_2O_{ppmv})^2} \tag{2}$$

Table 1 shows the coefficients of the humidity correction function obtained for each standard and each isotope.

A classical measurement sequence consists of 6 to 9 h of ambient air measurements, followed by successive measurements of each water standard for the calibration of the

ACPD
13, 30521–30574, 2013

system. The instrument is thus frequently calibrated at a given humidity level to correct data from a potential instrumental drift. However, a leak on one of the SDM syringes (from July 2012 to 21 February 2013, Table 2) constrained us to measure only one standard during a calibration sequence. For each injection of water standard (lasting 30 min), the isotopic measurements are integrated over the last 20 min to account for the stabilisation time of the system.

Figure 3 illustrates the humidity levels and the isotopic compositions of all calibrations during our observation period, averaged over this 20 min period, for the GREEN standard. The humidity level at which calibrations where performed has been modified several times. Initially, the aim was to make standard measurements at the same humidity level as ambient air, but the technical difficulties inherent to frequent adjusting of humidity level required us to rather use a constant humidity level. Figure 3 shows the raw measured humidity levels, whereas the isotopic composition values are corrected using Eq. (2) and reported for a constant humidity level of 10 000 ppmv. As seen on Fig. 3, there is no high frequency variability in water standard measurements. The typical variability timescale is above one week.

Unstabilities can occur if air bubbles are pertubating the liquid water delivery system of the SDM, or if the dry air flow is not stable. In order to validate calibrations sequences, an automatic criterion was applied to select stable standard measurements. This criterion is based on the standard deviations of the measurements of humidity, δ^{18}O and δD and depends on the mean humidity level (it was noticed that instabilities were in general higher for higher average humidity levels). Standard measurements are not taken into account if one of the standard deviation in δ^{18}O, δD or humidity level exceeds respectively 1‰, 6‰, and $\sigma_{\text{humidity, max}}$ (expressed in ppmv). $\sigma_{\text{humidity, max}}$ is empirically defined as:

$$\sigma_{\text{humidity, max}} = 0.043 \times \langle\text{humidity}\rangle + 57, \quad (3)$$

where $\langle\text{humidity}\rangle$ is the average humidity level during all the injection time.

ACPD
13, 30521–30574, 2013

Every single ambient air measurement is independently calibrated following a series of steps. After each water standard measurement no ambient air measurements is taken into account during 5.5 min (to avoid memory effects from the previous standard). For ambient air calibration, we search the two closest validated measurements of each water standard (one standard measurement prior and one standard measurement after the ambient air measurement). At least one of both standard measurements must be closer than 1.5 day from the ambient air measurement, otherwise this calibration is not used and the ambient air data are invalidated. The isotopic values of these standards measurements are first corrected using the humidity response function (Eq. 2) to the ambient air humidity level. Then, these two corrected standard measurements are interpolated at the time of the ambient air measurement. A linear regression curve is computed against their theoretical values, for each isotope. This regression is finally applied to calibrate the ambient air value.

2.5 Data gaps and data quality control

The instrument installation was completed on 21 September 2011. All experimental difficulties which occured until 31 May 2013 are summarized in Table 2. Several problems interrupted the water isotope monitoring and the performance of the calibration system, sometimes leading to data gaps over several months due to delays in shipping material to the station and to the low frequency of maintenance missions. On this 618 days period, we have validated water vapour isotopic measurements during 351 days (an overall performance of about 57 % in a semi-autonomous run).

The main issue identified here is a difference in the humidity response function for low humidity levels (< 2000 ppmv) obtained for the two water standards (Fig. 2). This is probably due to residual humidity in the dry air injected (through DRIERITE). This contrasts with other studies based on dry air from tank cylinders (Aemisegger et al., 2012). The impact of this process is detected for humidity < 4000 ppmv and is significant for humidity < 2000 ppmv. This calls for a cautious interpretation of ambient air data obtained at humidity < 2000 ppmv, which are only encountered episodically. During our

ACPD
13, 30521–30574, 2013

observation period, 3 % of hourly humidity measurements are below 2000 ppmv when isotopic measurements are available (distributed over 53 days).

Calibrations were conducted at low humidity levels (< 3000 ppmv) during April–June 2012 (Fig. 3). During this period, the standard deviation of each measurement is larger than for medium humidity levels (5000 to 10 000 ppmv). The humidity correction introduced a small but significant artefact on d measurements, as evidenced by systematic positive anomalies of the standard measurements (around 3 to 4 ‰), which may result in artificially depleted d measurements on this period.

The instrument stability can only be estimated through the repeatability of both calibration water standards measurements. The standard deviations of all water standards measurements are similar for both standards and are presented on Fig. 3 for GREEN standard. They are around 0.3‰ for δ^{18}O and 2.2‰ for δD, leading to a standard deviation of about 2.3‰ for d.

2.6 Independent humidity measurements

The Picarro humidity mixing ratio values are compared to those derived from the meteorological sensor relative humidity and temperature measurements. Hereafter, the humidity measurements are reported in water vapour molar mixing ratio (in $\mathrm{mmol_{water}\,mol^{-1}_{dry\ air}}$). As seen on Fig. 4, hourly averaged data from those two independent sensors over the full data sets from 21 September 2011 to 31 May 2013 are fitted by the following second order polynomial function with a high determination coefficient ($R^2 = 0.97$):

$$y = 0.013x^2 + 0.77x - 0.25, \tag{4}$$

where y gives meteorological sensor mixing ratio and x the Picarro mixing ratio.

In the 1 to 18 $\mathrm{mmol\,mol^{-1}}$ range, our comparison shows a non-linear relationship between the Picarro instrument and the meteorological sensor. Earlier studies have reported different results when comparing Picarro measurements with independent

ACPD
13, 30521–30574, 2013

humidity observations. Aemisegger et al. (2012) showed a linear response of the analyzers using a dew point generator to control humidity level on a 4 to 31 mmol mol^{-1} range. Tremoy et al. (2011) showed a non-linear response of the analyzer compared to humidity based on meteorological sensor temperature and relative humidity observations, on a 5 to 36 mmol mol^{-1} range.

In order to report humidity when the Picarro is not working, the meteorological sensor data are homogenised using Eq. (4). Our final humidity dataset is composed of an average of Picarro and meteorological sensor corrected values.

2.7 Lagrangian moisture source diagnostic

The origin and transport of water vapour to Ivittuut is studied using a Lagrangian moisture source diagnostic (Sodemann et al., 2008b). Air parcels are traced backward from a box over Ivittuut (61.0° N, 48.9° W to 61.4° N, 47.8° W and from 0 to 500 m a.g.l.) with a 3 h timestep for 10 days. Parcel trajectories have been calculated using the FLEXPART model v8.1 (Stohl et al., 2005), forced by ECMWF ERA-Interim reanalysis data, similar to the setup described in Sodemann and Stohl (2009). Moisture origin is then diagnosed from specific humidity increases from one time step to the next along the air parcel trajectories, and made quantitative by relating the increase to the total humidity in the air parcel, and any precipitation events occurring en route. Further details on the method are available in Sodemann et al. (2008b).

From this water transport simulation, the "moisture uptake" is computed as the amount of water injected in the air masses within the boundary layer then going to Ivittuut for each horizontal grid cell, and reported in mm/day. It can be interpreted as the contribution of total evaporation at the moisture sources to water vapour in Ivittuut.

2.8 Water isotope enabled AGCM

The use of an isotope enabled AGCM provides us with additional large scale information for interpretation of our local observations. Simulations of atmospheric wa-

ACPD
13, 30521–30574, 2013

ter vapour isotopic composition are extracted from the isotope enabled version of LMDZ4 (Hourdin et al., 2006), named LMDZiso and developed at the Laboratoire de Météorologie Dynamique (LMD) by Risi et al. (2010a). Model inter-comparisons conducted against data acquired at NEEM showed that the performance of LMDZiso is similar to that of other models at the seasonal and inter-annual scales (Steen-Larsen et al., 2011, 2013a). It has been used over Greenland by Casado et al. (2012) to assess the impact of precipitation intermittency on NAO-temperature signals and by Ortega et al. (2013) to characterize the influence of weather regimes on ice core signals.

The model has a uniform resolution of 3.75° in longitude and 2.5° in latitude and 19 vertical levels. The simulation was nudged by three-dimensional fields of horizontal winds of ECMWF operational analyses for the period after 2002, and of ERA-40 for the period 1961–1974, ensuring realistic synoptic and long term variability. Risi et al. (2010a) observed no noticeable discontinuity linked to the change of nudging atmospheric data.

Daily outputs, for comparison with Ivittuut observations, are provided for the September 2011 to December 2012 period. Monthly outputs over the 1961–1974 period are used for comparison with GNIP/IAEA data presented in Supplement Sect. A. Hereafter, grid cell coordinates correspond to the western border of the cell for longitudes, and to the center of the cell for latitudes (LMDZiso model convention). For the comparison of daily outputs with Ivittuut observations (Sect. 4.1), we use LMDZiso model outputs from two different grid cells: the ice sheet grid cell closest to the station (62.11° N, 48.75° W), hereafter called "Ivittuut terrestrial grid cell", and the nearest oceanic grid cell (62.11° N, 52.5° W) located in the Labrador sea, hereafter called "nearest oceanic grid cell".

3 Results: water isotopes, local climate and moisture transport

Hourly averaged measurements of δD_v and $\delta^{18}O_v$ over the complete observation period show a slope of 6.8 ‰‰$^{-1}$ (R^2 = 0.97; N = 7889), comparable to the 6.5 ‰‰$^{-1}$ value reported by Steen-Larsen et al. (2013a) for central Greenland in summer.

ACPD
13, 30521–30574, 2013

Figure 5 presents the time-series of all validated hourly observations at Ivittuut station. We observe small diurnal variations in summer (Sect. 3.1). Synoptic variations are reported throughout the year on meteorological parameters and isotopes (Sect. 3.2), with particularly strong heat waves in summer 2012 (Sect. 3.3). Seasonal variations with similar magnitudes as synoptic variations are observed with different timings of extrema for $\delta^{18}O_v$ and d_v (Sect. 3.4). Given the length of our record, the seasonal cycle is affected by the particular events occuring during the year.

The water vapour isotopic content variations are compared to variations of precipitation isotopic content in Sect. 3.5. Then, the statistical relationships between Ivittuut water vapour isotopic composition and meteorological parameters are described in Sect. 3.6.

3.1 Diurnal variability

During summer months (June to August), a diurnal cycle is observed in humidity mixing ratio, $\delta^{18}O_v$ and d_v when no large pressure change is observed. This was the case during 35 days in summer 2012 from June to August (16 June to 28, 16 July to 20, 22 to 27 July and 14 August to 26). Figure 5f–j depicts a zoom on the 21 to 23 August 2012, where diurnal cycle is observed. The amplitude of the diurnal cycle is of about 1 mmol mol^{-1} on humidity mixing ratio, 1‰ on $\delta^{18}O_v$ and 5‰ on d_v. The minima and maxima occur respectively around 08:00 and 18:00 UTC (05:00 and 15:00 LT) for temperature and humidity mixing ratio, at 00:00 and 12:00 UTC (21:00 and 09:00 LT) for $\delta^{18}O$, and at 00:00 and 18:00 UTC (21:00 and 15:00 LT) for d_v.

These amplitudes of diurnal variations are on the same order of magnitude as those found by Welp et al. (2012) for six mid-latitude continental sites in different environments (forest, urban, grassland and agricultural land). Welp et al. (2012) linked the diurnal variations to plant transpiration and boundary layer dynamics. The amplitudes of diurnal variation are also similar to those of Steen-Larsen et al. (2013a) at the NEEM site in terms of d_v, but lower for humidity and $\delta^{18}O$. For the NEEM site, these variations are attributed to exchanges of humidity between the air and the snow surface, and also

ACPD
13, 30521–30574, 2013

boundary layer dynamics. In our case, the effects of surface fluxes (plant transpiration, snow–air exchanges) are probably less important than the influence of the advection of marine humidity. Further analysis of the boundary layer processes are limited by the lack of monitoring of the boundary layer height.

The diurnal cycle is generally smaller than the day to day variations which are governed by large scale advection processes.

3.2 Synoptic timescale variability and moisture source diagnostic

In this section, we focus on the variations occuring at a timescale of a few days (synoptic events). Several events of humidity increase were observed, related to low pressure systems. We selected 14 events based on an automatic criterion of humidity increase higher than 3 mmol mol^{-1} within two days. One event was selected in summer season, 5 events in autumn, 4 in winter and 4 in spring. Figure 6 presents the time series of meteorological and isotopic anomalies during 4 days surrounding each event. A composite synoptic event is calculated as an aggregation of all events (black line on Fig. 6). This composite event depicts an increase in temperature (+7 °C), humidity (+4 mmol mol^{-1}) and isotopes (+5‰ in $\delta^{18}O_v$) as well as a decrease in atmospheric pressure (−9 hPa) and in d_v (−15‰).

Figure 7 presents the average daily moisture uptake and the averaged sea level pressure, from D-3 to D+1, where D+0 corresponds to the events. The same time scale is used as for the composite series of Fig. 6. These events correspond to the arrival of a low pressure system in Southern Greenland (see mean sea level pressure map, Fig. 7). At D-3, moisture is mainly coming from Northern Atlantic (around Iceland) and Labrador sea. Between D-2 and D+0, there is a strong increase in moisture uptake further south over the Atlantic ocean, along the low pressure cell. At D+1, this southern moisture uptake vanishes, and the influence of Northern Atlantic and Labrador sea sources is increasing again. The change in moisture origin observed during these high humidity spike probably explains the large variability of d_v values. Section 4.4 investi-

ACPD
13, 30521–30574, 2013

gates the relationship between d_v and surface climate in the area of strong moisture uptake in the Atlantic (south of Greenland).

3.3 Summer 2012 heat wave

In summer 2012, successive strong heat waves have been observed in Ivittuut (Fig. 5) and over all Greenland, which led to a record melt of the Greenland ice sheet due to positive snow albedo and liquid cloud feedbacks (Fettweis et al., 2013; Bennartz et al., 2013; Nghiem et al., 2012; Neff et al., 2013). During these events, very high humidity spikes are also encountered, whereas the associated signal of $\delta^{18}O_v$ is flat. Moisture source analysis (not shown here) reveal that these events are associated with dry air coming from North America, shifting towards the Western subtropical Atlantic and towards southern Greenland. The Greenland melt event is therefore associated with a long distance transport path, associated with onway distillation and leading to relatively low $\delta^{18}O_v$ levels despite high local humidity values. These events will be investigated more in details in a forthcoming paper.

3.4 Seasonal variability and moisture source diagnostic

The mean values of $\delta^{18}O_v$ and d_v computed from full hourly data record are respectively of −22.7‰ and 13.6‰. From monthly averaged values of $\delta^{18}O_v$ and d_v presented in Table 3, we observe a seasonal amplitude of 10.3‰ for $\delta^{18}O_v$ and 20.2‰ for d_v. Minima in $\delta^{18}O_v$ are observed in November–December, while maxima occur in June–July. Regarding d_v, minimum values are in May–June and maximum in November. During autumn periods, $\delta^{18}O_v$ and d_v values are respectively approximately 5‰ below and 6 to 12‰ above long term mean values. Those extreme values are not always simultaneous. In 2011, extrema in $\delta^{18}O_v$ and d_v were both observed in November, whereas in 2012, they were respectively observed in December and November (Fig. 5d and e).

ACPD
13, 30521–30574, 2013

Moisture source diagnostic over the four seasons in 2012 (Fig. 8) highlight seasonal shifts of moisture sources for Ivittuut, potentially influencing the observed water vapour isotopic signal in Ivittuut. In winter, sources are centered in the North Atlantic, south of Greenland. In spring and autumn, moisture also originates from the North American continent, together with a larger contribution from the subtropical ocean. In summer, the dominant moisture sources appear to be North-Eastern America and South Greenland. This is consistent with long distance transport from North America to Southern Greenland identified in summer from pollen observations by Rousseau et al. (2003). Along trajectories from North America to the Atlantic Ocean, dry autumn air masses (compared to summer where evapotranspiration is more intense) could cause enhanced kinetic fractionation and contribute to the observed autumnal maximum in d_v. High d_v values in autumn have already been observed in Arctic water vapour (Kurita, 2011), attributed to oceanic evaporation at the sea–ice border.

This motivates further investigation of relationships between water vapour isotopes and local climate season by season as described in Sect. 3.6.

3.5 Precipitation isotopic composition and equilibrium with vapour

For precipitation measurements, the relationship between δD_p and $\delta^{18}O_p$ is characterised by a slope of 7.5 ‰‰$^{-1}$ ($R^2 = 0.92$, $N = 39$).

We want to infer if the water vapour is in isotopic equilibrium with the precipitation and is thus representative of the vapour used to form condensates. As described in Sect. 2.3, a theoretical water vapour isotopic composition is calculated from precipitation isotopic results, supposing phase change at equilibrium. Figure 9 presents the time series of the isotopic composition of the observed precipitation (noted with suffix p), together with the observed water vapour (noted in this section with suffix v, obs) and with water vapour calculated at equilibrium with precipitation data (noted with suffix v, eq), from November 2011 to December 2012.

ACPD
13, 30521–30574, 2013

Concerning precipitation isotopic measurements, $\delta^{18}O_p$ values are in the range of −20 to −5‰, with quite low values compared to the GNIP/IAEA mean seasonal cycle (described in Supplement Sect. A). d_p varies from about −5 to +20‰, with higher values for snow samples in autumn 2011, compared to the climatological average. During winter time, snow precipitation samples show generally higher d_p than liquid precipitation, reflecting the different equilibrium fractionation coefficients for solid or for liquid phases.

$\delta^{18}O_{v,\,obs}$ and $\delta^{18}O_{v,\,eq}$ time series appear very consistent. A clear seasonal cycle can be seen on $\delta^{18}O_{v,\,eq}$, with more depleted values in winter than in summer, consistent with the $\delta^{18}O_{v,\,obs}$ seasonal cycle. The rather flat seasonal cycle on GNIP/IAEA and on our precipitation $\delta^{18}O_p$ data (described in Supplement Sect. A) can be explained by a strong seasonal cycle in vapour $\delta^{18}O_v$ which would be partly erased by the impact of temperature on vapour to solid fractionation. $d_{v,\,eq}$ confirms the seasonal cycle reflected in $d_{v,\,obs}$, with peak values in autumn. We note that a one month lag between d and $\delta^{18}O$ of central Greenland surface snow had been depicted in shallow ice core seasonal cycles (Hoffmann et al., 1998). However, diffusion processes may affect the ice core record (Johnsen et al., 2000), which is not the case for our measurements. We finally note that the observed water vapour $d_{v,\,obs}$ is located in-between the theoretical values derived from liquid and solid samples.

We conclude from this comparison that surface water vapour may be at equilibrium with precipitation. While such equilibrium may arise from exchanges between rainfall and surface vapour, we cannot rule out that surface vapour may also be representative from moisture at the cloud altitude. This would be compatible with the predominance of low altitude clouds in our observation region and the Northern Atlantic region (Liu et al., 2012).

ACPD
13, 30521–30574, 2013

3.6 Statistical relationships between water vapour isotopes and local climate

We now explore the relationships between $\delta^{18}O_v$ and local climate parameters on different timescales. In this subsection, linear statistical analyses are conducted, and correlation coefficients (R) and slopes are reported (see Table 4).

From all daily data, the linear regression between $\delta^{18}O_v$ and local temperature gives a low slope of 0.37 ‰ °C^{-1} ($R = 0.65$, $N = 282$, see Fig. 10a). Note that, for Rayleigh distillation, the slope between water vapour and temperature is very close to the slope between precipitation isotopic composition and temperature. For Ivittuut, the slope obtained for vapour is at the lowest end of the slopes usually obtained for precipitation $\delta^{18}O$ and temperature relationships: for ice core reconstructed $\delta^{18}O$ and temperatures (Vinther et al., 2010; Masson-Delmotte et al., 2011; Kindler et al., 2013), or for isotopically enabled atmospheric models simulations (Sime et al., 2013). It is also two times lower than the spatial relationship observed on the Greenland ice sheet (Sjolte et al., 2011). A stronger linear correlation is observed between $\delta^{18}O_v$ and humidity mixing ratio w over the complete serie ($R = 0.78$, $N = 351$, Fig. 10c). The best correlation with humidity is obtained using a log-linear relationship ($R = 0.82$, $N = 351$). The corresponding regression equation giving $\delta^{18}O_v$ in ‰ as a function of w in mmol mol^{-1} is:

$$\delta^{18}O_v = -33.0 + 5.9 \ln(w) \quad (5)$$

This result is consistent with Rayleigh distillation during air masses advection, with similar coefficients as calculated by Lee et al. (2006) for one year observation period in New Haven.

Beyond the correlation between $\delta^{18}O$ and Ivittuut relative humidity ($R = 0.62$, $N = 282$), we observe that, for a given level of humidity, $\delta^{18}O$ is higher in spring–summer and more depleted in autumun–winter (Fig. 10c, e and g). Moreover, seasonal maxima and minima do not occur in phase for $\delta^{18}O$ and local relative humidity.

Within a given season, we explore the relationships (see Table 4) between water isotopes and local climate after detrending to remove seasonal effects (anomalies are

ACPD
13, 30521–30574, 2013

computed against 15 day running average). The relationships are computed for the four seasons, based on daily averaged values: Spring (March, April, May), Summer (June, July, August), Autumn (September, October, November), Winter (December, January, February). We first observe a strong correlation between $\delta^{18}O_v$ and temperature in autumn ($R = 0.63$, $N = 67$, slope 0.7 ‰ °C^{-1}) which is weaker in spring and vanishes in summer and winter. The relationship between $\delta^{18}O_v$ and the logarithm of specific humidity is more robust throughout autumn, winter and spring than during summer, where we have reported a decoupling during the heat wave event (see also Sect. 3.3). A strong anti-correlation between d_v and $\delta^{18}O_v$ is seen in spring, summer and autumn, but is reduced in winter. We conclude from Table 4 that the strongest correlations between $\delta^{18}O_v$ and temperature or the logarithm of humidity and between d_v and relative humidity are observed in autumn, marked by large amplitude synoptic events. Note that the relationship between d_v and North Atlantic relative humidity is investigated in Sect. 4.4.

Interestingly, the statistical relationships observed in autumn are also closest to those extracted from the composite synoptic event, based on hourly averaged values (Table 4, Sect. 3.2). The overall correlations reported from all daily data therefore combine two effects, one linked with seasonal cycles and another one linked with synoptic events (with higher $\delta^{18}O_v$-temperature slopes), clearly visible within autumn data. Longer records will be needed to deconvolve these two effects.

Finally, we note that different patterns emerge from diurnal cycles, based on hourly averaged data, where our statistical analysis only reveals a significant anti-correlation between d_v and $\delta^{18}O_v$.

4 Discussion: comparison with LMDZiso simulations

In this section, Ivittuut observations are confronted to LMDZiso simulations in order to: test the realism of these simulations, provide large scale information for the interpretation of our observations and estimate the spatial representativeness of our ob-

ACPD
13, 30521–30574, 2013

servations. The comparison of LMDZiso and GNIP/IAEA climatologies (presented in Supplement Section A) shows that LMDZiso has a cold bias and overestimates precipitation amount. For precipitation isotopic composition, the simulated $\delta^{18}O_p$ values are too depleted, consistent with climate biases. Moreover, LMDZiso strongly underestimates the magnitude of d_p seasonal variations.

Section 4.1 compares our observations with outputs from the model first vertical level. Section 4.2 is dedicated to relationships between simulated water vapour and local climate variables. Section 4.3 investigates the spatial representativeness of our observations, and Sect. 4.4 focuses on the influence of relative humidity at the moisture source on d_v.

4.1 Comparison of LMDZiso bottom layer isotopic composition with Ivittuut observations at synoptic and seasonal scales

Figure 11 presents the daily averaged time series of Ivittuut observations, compared to both oceanic and Ivittuut terrestrial grid cells model output.

The Ivittuut terrestrial grid cell shows a cold and dry bias (in terms of w), explained by the grid size covering part of the ice cap. The nearest oceanic grid cell represents well temperature and humidity mean levels and seasonal cycles, with smaller temperature variability linked with ocean inertia. For $\delta^{18}O_v$, the variations of both model grid cells are close, but the magnitude of these variations are larger on the Ivittuut terrestrial grid cell. The seasonal variability is better represented by the Ivittuut terrestrial grid cell. The oceanic grid cell shows too smooth $\delta^{18}O_v$ variations, possibly due to insufficient distillation (driven by air temperature variations). For both model grid cells, LMDZiso strongly underestimates the synoptic and seasonal variability of d_v. This was also observed at NEEM site by Steen-Larsen et al. (2013a) for Arctic air masses and in Saclay (France, 20 km southwest of Paris) by Risi et al. (2010a).

For all parameters except d_v, the synoptic variability is well represented by the Ivittuut terrestrial grid cell. For some periods (25 October to 5 November 2011 and 11 to 27 August 2012), the discrepancies between Ivittuut terrestrial grid cell and observations

ACPD
13, 30521–30574, 2013

increase and the variations are better represented by the nearest oceanic grid cell, or eventually by a weighted average of both nearest oceanic and Ivittuut terrestrial grid cells. This highlights the need for downscaling methodologies in order to make best use of such station data. Simulations performed at a spatial resolution smaller than the distance from the ocean to the ice cap (~ 20 km) would help solving this problem.

4.2 Statistical relationships with local climatic parameters in LMDZiso

The correlations between isotopic values and local meteorological parameters have been computed from daily LMDZiso outputs at the Ivittuut terrestrial grid cell from 21 september 2011 to 31 December 2012, for comparison with correlations obtained for observations (see Sect. 3.6). These correlations are presented for the whole dataset in the rightmost column of Table 4.

The δD_v-$\delta^{18}O_v$ slope (not presented in Table 4) is higher in LMDZiso simulations than in observations (7.5 for LMDZiso against 6.8 ‰‰$^{-1}$ for observations) and the correlation is similar ($R^2 = 0.99$, $N = 488$ in LMDZiso). The $\delta^{18}O_v$-w relationship in the model is best reproduced by a log-linear function ($R = 0.7$, $N = 467$), as seen for observations, reproducing the influence of Rayleigh distillation on $\delta^{18}O_v$, although with a lower slope than observed.

We have already seen that LMDZiso underestimate d_v variability. As a result, the relationships between d_v in LMDZiso and other parameters lead to lower slopes compared to observations. The correlation becomes low with temperature and w, compared to observations. The model nevertheless produces a strong anti-correlation between d_v and $\delta^{18}O_v$, although with a lower slope (−0.55 ‰‰$^{-1}$) than observed.

4.3 Spatial representativeness of Ivittuut observations in LMDZiso

Figure 12 shows correlation coefficients maps between Ivittuut observations and model outputs of surface air temperature, relative humidity, $\delta^{18}O_v$ and d_v, calculated from daily values from 21 September 2011 to 31 December 2012. For temperature and

ACPD
13, 30521–30574, 2013

$\delta^{18}O_v$, the correlations are high at Ivittuut terrestrial grid cell ($R = 0.91$, $N = 212$ and $R = 0.63$, $N = 219$ respectively) and over all Greenland. For $\delta^{18}O_v$, the correlation abruptly disappear at the nearest oceanic grid cell ($R = -0.21$, $N = 219$), consistent with the different behaviours between oceanic and continental grid cells, as previously seen from Fig. 11. The reason for this strong spatial structure remains unexplained. Concerning relative humidity and d_v, the maxima of correlation between the model and our observations are not located around the station, but over the Atlantic ocean, on the region represented by the blue square on Fig. 12 (lower right box). Hereafter, we call "Zone 1", this Atlantic region going from 49.44° N, 41.25° W to 59.58° N, 22.5° W approximately. From FLEXPART backtrajectories, we had seen that this region of high correlation is an important moisture source for our station (Figs. 7 and 8). The next section focuses on the impact of this region meteorological conditions on Ivittuut d_v.

4.4 Relationships between deuterium excess and North Atlantic surface relative humidity

Here, we investigate the relationships between Zone 1 relative humidity (normalised to SST, from LMDZiso data) and Ivittuut d_v (from observations and LMDZiso), summarized in Table 5. The observations show that d_v is closely related to relative humidity of Zone 1 (with a slope of $-1.1\,‰\,\%^{-1}$). This result is confirmed when using relative humidity from ECMWF data (not shown here). This slope is higher than the theoretical value (Merlivat and Jouzel, 1979) and the global empirical relationship observed from other studies (Pfahl and Sodemann, 2013). We have computed the correlation of d_v observed at Ivittuut with relative humidity in Zone 1, applying different time lags (−5 to +5 days). The best result is obtained when no lag time in applied. We conclude that the transport of the signal from Zone 1 to Ivittuut occurs in less than 24 h, consistent with FLEXPART backtrajectory analyses.

In LMDZiso, d_v in Zone 1 is closely anti-correlated with relative humidity at the ocean surface (with a slope of $-0.5\,‰\,\%^{-1}$). This is consistent with theoretical behavior of

ACPD
13, 30521–30574, 2013

evaporation. However, this link between the simulated d_v and Zone 1 relative humidity is lost during transportation to Ivittuut, as illustrated by the weak correlation between d_v simulated at Ivittuut and both Zone 1 relative humidity ($R = -0.28$) and Ivittuut observed d_v ($R = 0.37$). We therefore infer that LMDZiso loses part of d_v source signal until air masses reach Ivittuut.

Figure 13 illustrates the fact that seasonal and synoptic variations of relative humidity in Zone 1 may explain the seasonal cycle of Ivittuut d_v and its lag with respect to the seasonal cycle of $\delta^{18}O_v$ or climate variables in Ivittuut, as well as its minimum summer variability. Half of d_v variance can be explained by the variability of Zone 1 relative humidity.

Altogether, we know (i) that the strong correlation between observed d_v and relative humidity of Zone 1 suggests a key role for this source area; (ii) there are significant changes in moisture sources for Ivittuut, both at synoptic and seasonal scales (Sects. 7 and 8); (iii) despite biases of LMDZiso for d_v, the spatial distribution of simulated d_v (see d_v maps issued from LMDZiso outputs in Supplement Fig. B.2) suggests that Arctic moisture is characterized by very high d_v in autumn; (iv) changes in the fraction of North Atlantic vs. Arctic moisture therefore contribute to the full magnitude of d_v variability at Ivittuut. If LMDZiso does not resolve these source changes properly, d_v variations could be underestimated. The effect of horizontal mixing between different sources might also play an important role in the final Ivittuut d_v signal. A misrepresentation of horizontal mixing could be linked with the model resolution, as highlighted by Werner et al. (2011) for Antarctica. In our case, small scale storms channelled along the south Greenland coast are not resolved at the model resolution.

Our analysis confirms other studies suggesting that Atmospheric General Circulation Models fail to reproduce the magnitude of synoptic and seasonal d_v variations in Greenland Steen-Larsen et al. (2013a); Sjolte et al. (2011); Werner et al. (2011), and calls for a careful use of such model results for the quantitative interpretation of ice core records.

ACPD
13, 30521–30574, 2013

5 Conclusions

We have reported here a year-round monitoring of water vapour isotopic composition conducted in semi-autonomous conditions in southern Greenland, with only annual maintenance. After a first adjustement phase where data acquisition was interrupted by a storm and problems with the calibration system, the system has been fully operational. The accuracy of the validated data (0.3‰ for δ^{18}O, 2.2‰ for δD and 2.3‰ for d) is sufficient to resolve diurnal, synoptic and seasonal variations in $\delta^{18}O_v$ and d_v. The small diurnal cycle suggests limited effects of local processes (such as evapotranspiration, boundary layer dynamics) and the comparison between our data, backtrajectory calculations and LMDZiso simulations confirms that the surface vapour isotopic composition is reflecting changes in large scale moisture advection.

For $\delta^{18}O_v$, our data show that its variability is strongly driven by changes in local air temperature and humidity, as expected from Rayleigh distillation. However, we observe relatively small $\delta^{18}O_v$-T slopes (0.37 ‰ °C^{-1}) and changing relationships through seasons, likely due to seasonal shifts of moisture sources. Temperature variations only explain at best (in autumn) half of $\delta^{18}O_v$ variance. We report specifically a divergence between $\delta^{18}O_v$ and temperature during the summer 2012 heat wave, associated with long distance transport from an exceptional atmospheric river. The comparison between the isotopic measurements at Ivittuut with those acquired above the ice sheet (e.g. NEEM, Steen-Larsen et al., 2013a) will offer an isotopic benchmark to test the parameterisations of atmospheric models for this event.

Based on vapour measurements and vapour calculated at equilibrium from precipitation isotopic composition measurements, we identify a difference in the seasonal cycle of $\delta^{18}O_v$ (in phase with local temperature) and d_v. Beyond an anti-phase with $\delta^{18}O_v$ at the synoptic scale, d_v is minimum in spring and maximum in autumn. Variations of d_v appear strongly correlated at the synoptic and seasonal scale with relative humidity at the surface of a North Atlantic area, south of Iceland. Calculated from FLEXPART, moisture sources are identified in the Labrador Sea, the subtropical Atlantic and the

ACPD
13, 30521–30574, 2013

North Atlantic. Shifts in evaporation conditions probably explain the variance of $\delta^{18}O_v$ which is not linearly related to Ivittuut meteorological data (temperature and humidity), and deviations from slopes expected from pure Rayleigh distillations.

The response function of the measurements against humidity suggests artefacts due to the use of DRIERITE in our introduction system, for low humidity levels. While it does not impact the results reported here, further studies would benefit from an alternative calibration method using e.g. dry air cylinders.

Testing the robustness of our findings (such as the d_v peak in autumn) over longer time periods motivates an extension of the surface water vapor monitoring in Ivittuut over several years. This would allow to investigate the local fingerprint of changes in weather regimes and explore inter-annual variations.

The mismatch between LMDZiso simulated d_v and our data should be further investigated. The fact that LMDZiso simulates too small d_v variations at Ivittuut could be linked either to an underestimation of the variability of d_v at the moisture source and/or to an inadequate representation of the moisture sources mixing. A first test could be to run simulations at higher resolution, in order to explore how changes in model resolution would impact moisture transportation, as small scale storms are known to transport moisture from the North Atlantic, below Iceland, towards south Greenland. A second test would be to investigate the isotopic signal associated with different moisture sources, using water tagging diagnostics (Risi et al., 2010b). This model-data comparison would benefit from similar comparisons with water vapour measurements from other locations along North Atlantic/Arctic air mass trajectories, especially in locations close to moisture sources, such as Bermuda (H. C. Steen-Larsen, personal communication, 2013).

Supplementary material related to this article is available online at http://www.atmos-chem-phys-discuss.net/13/30521/2013/acpd-13-30521-2013-supplement.zip.

ACPD
13, 30521–30574, 2013

Acknowledgements. A precious logistic help has been provided to the station by Grønlands Kommando from Grønnedal military base since 2007. We greatly want to thank them for this very fruitful collaboration. We also acknowledge Sonia Falourd and Bénédicte Minster for the isotopic measurements of precipitation samples. We finally warmly acknowledge the helpful comments and suggestions of Amaelle Landais, Guillaume Tremoy and Françoise Vimeux. LMDZ simulations were performed on the NEC supercomputer of the IDRIS computing center. This research was funded by the ANR CEPS *Green Greenland* project (grant number ANR-10-CEPL-0008). Ivittuut station is funded by IPEV, CARBOOCEAN, ICOS.

The publication of this article is financed by CNRS-INSU.

References

Aemisegger, F., Sturm, P., Graf, P., Sodemann, H., Pfahl, S., Knohl, A., and Wernli, H.: Measuring variations of δ^{18}O and δ^{2}H in atmospheric water vapour using two commercial laser-based spectrometers: an instrument characterisation study, Atmos. Meas. Tech., 5, 1491–1511, doi:10.5194/amt-5-1491-2012, 2012. 30525, 30530, 30532, 30534

Bennartz, R., Shupe, M. D., Turner, D. D., Walden, V. P., Steffen, K., Cox, C. J., Kulie, M. S., Miller, N. B., and Pettersen, C.: July 2012 Greenland melt extent enhanced by low-level liquid clouds, Nature, 496, 83–86, doi:10.1038/nature12002, 2013. 30526, 30538

Casado, M., Ortega, P., Masson-Delmotte, V., Risi, C., Swingedouw, D., Daux, V., Genty, D., Maignan, F., Solomina, O., Vinther, B., Viovy, N., and Yiou, P.: Impact of precipitation intermittency on NAO-temperature signals in proxy records, Clim. Past, 9, 871–886, doi:10.5194/cp-9-871-2013, 2013. 30524, 30535

Craig, H. and Gordon, L. I.: Deuterium and oxygen 18 variations in the ocean and the marine atmosphere, Consiglio nazionale delle richerche, Laboratorio de geologia nucleare, Stable Isotopes in Oceanographic Studies and Paleotemperatures, 161–182, 1965. 30524

Cuffey, K. M., Alley, R. B., Grootes, P. M., and Anandakrishnan, S.: Toward using borehole temperatures to calibrate an isotopic paleothermometer in central Greenland, Global Planet. Change, 6, 265–268, doi:10.1016/0921-8181(92)90042-9, 1992. 30524

Dahl-Jensen, D., Mosegaard, K., Gundestrup, N., Clow, G. D., Johnsen, S. J., Hansen, A. W., and Balling, N.: Past temperatures directly from the Greenland ice sheet, Science, 282, 268–271, doi:10.1126/science.282.5387.268, PMID: 9765146, 1998. 30524

Dahl-Jensen, D., Albert, M. R., Aldahan, A., Azuma, N., Balslev-Clausen, D., Baumgartner, M., Berggren, A.-M., Bigler, M., Binder, T., Blunier, T., Bourgeois, J. C., Brook, E. J., Buchardt, S. L., Buizert, C., Capron, E., Chappellaz, J., Chung, J., Clausen, H. B., Cvijanovic, I., Davies, S. M., Ditlevsen, P., Eicher, O., Fischer, H., Fisher, D. A., Fleet, L. G., Gfeller, G., Gkinis, V., Gogineni, S., Goto-Azuma, K., Grinsted, A., Gudlaugsdottir, H., Guillevic, M., Hansen, S. B., Hansson, M., Hirabayashi, M., Hong, S., Hur, S. D., Huybrechts, P., Hvidberg, C. S., Iizuka, Y., Jenk, T., Johnsen, S. J., Jones, T. R., Jouzel, J., Karlsson, N. B., Kawamura, K., Keegan, K., Kettner, E., Kipfstuhl, S., Kjær, H. A., Koutnik, M., Kuramoto, T., Köhler, P., Laepple, T., Landais, A., Langen, P. L., Larsen, L. B., Leuenberger, D., Leuenberger, M., Leuschen, C., Li, J., Lipenkov, V., Martinerie, P., Maselli, O. J., Masson-Delmotte, V., McConnell, J. R., Miller, H., Mini, O., Miyamoto, A., Montagnat-Rentier, M., Mulvaney, R., Muscheler, R., Orsi, A. J., Paden, J., Panton, C., Pattyn, F., Petit, J.-R., Pol, K., Popp, T., Possnert, G., Prié, F., Prokopiou, M., Quiquet, A., Rasmussen, S. O., Raynaud, D., Ren, J., Reutenauer, C., Ritz, C., Röckmann, T., Rosen, J. L., Rubino, M., Rybak, O., Samyn, D., Sapart, C. J., Schilt, A., Schmidt, A. M. Z., Schwander, J., Schüpbach, S., Seierstad, I., Severinghaus, J. P., Sheldon, S., Simonsen, S. B., Sjolte, J., Solgaard, A. M., Sowers, T., Sperlich, P., Steen-Larsen, H. C., Steffen, K., Steffensen, J. P., Steinhage, D., Stocker, T. F., Stowasser, C., Sturevik, A. S., Sturges, W. T., Sveinbjörnsdottir, A., Svensson, A., Tison, J.-L., Uetake, J., Vallelonga, P., van de Wal, R. S. W., van der Wel, G., Vaughn, B. H., Vinther, B., Waddington, E., Wegner, A., Weikusat, I., White, J. W. C., Wilhelms, F., Winstrup, M., Witrant, E., Wolff, E. W., Xiao, C., and Zheng, J.: Eemian interglacial reconstructed from a Greenland folded ice core, Nature, 493, 489–494, doi:10.1038/nature11789, 2013. 30524

Dansgaard, W.: Stable isotopes in precipitation, Tellus, 16, 436–468, doi:10.1111/j.2153-3490.1964.tb00181.x, 1964. 30524

Fettweis, X., Hanna, E., Lang, C., Belleflamme, A., Erpicum, M., and Gallée, H.: *Brief communication* "Important role of the mid-tropospheric atmospheric circulation in the recent surface

ACPD
13, 30521–30574, 2013

melt increase over the Greenland ice sheet", The Cryosphere, 7, 241–248, doi:10.5194/tc-7-241-2013, 2013. 30526, 30538

Gribanov, K., Jouzel, J., Bastrikov, V., Bonne, J.-L., Breon, F.-M., Butzin, M., Cattani, O., Masson-Delmotte, V., Rokotyan, N., Werner, M., and Zakharov, V.: ECHAM5-wiso water vapour isotopologues simulation and its comparison with WS-CRDS measurements and retrievals from GOSAT and ground-based FTIR spectra in the atmosphere of Western Siberia, Atmos. Chem. Phys. Discuss., 13, 2599–2640, doi:10.5194/acpd-13-2599-2013, 2013. 30526, 30529

Guillevic, M., Bazin, L., Landais, A., Kindler, P., Orsi, A., Masson-Delmotte, V., Blunier, T., Buchardt, S. L., Capron, E., Leuenberger, M., Martinerie, P., Prié, F., and Vinther, B. M.: Spatial gradients of temperature, accumulation and δ^{18}O-ice in Greenland over a series of Dansgaard–Oeschger events, Clim. Past, 9, 1029–1051, doi:10.5194/cp-9-1029-2013, 2013. 30524

Hoffmann, G., Stievenard, M., Jouzel, J., White, J., and Johnsen, S.: Deuterium excess record from central Greenland: modeling and observations, in: International Symposium on Isotopes Techniques in the Study of Past and Current Environmental changes in the Hydrosphere and the Atmosphere, IAEA, Vienna, 14–18 April 1997, 591–602, 1998. 30540

Hourdin, F., Musat, I., Bony, S., Braconnot, P., Codron, F., Dufresne, J.-L., Fairhead, L., Filiberti, M.-A., Friedlingstein, P., Grandpeix, J.-Y., Krinner, G., LeVan, P., Li, Z.-X., and Lott, F.: The LMDZ4 general circulation model: climate performance and sensitivity to parametrized physics with emphasis on tropical convection, Clim. Dynam., 27, 787–813, doi:10.1007/s00382-006-0158-0, 2006. 30535

Jacob, H. and Sonntag, C.: An 8-year record of the seasonal variation of ^{2}H and ^{18}O in atmospheric water vapour and precipitation at Heidelberg, Germany, Tellus B, 43, 291–300, doi:10.1034/j.1600-0889.1991.t01-2-00003.x, 1991. 30525

Johnsen, S. J.: Stable isotope homogenization of polar firn and ice, in: Isotopes and Impurities in Snow and Ice, 210–219, I.U.G.G. XVI, General Assembly, Grenoble August/September, 1975, IAHS-AISH Publ. 118, Washington D.C., 1977. 30524

Johnsen, S. J., Clausen, H. B., Cuffey, K. M., Hoffmann, G., Schwander, J., and Creyts, T.: Diffusion of stable isotopes in polar firn and ice: the isotope effect in firn diffusion, Phys. Ice Core Rec., 159, 121–140, 2000. 30540

Jouzel, J.: Water stable isotopes: atmospheric composition and applications in polar ice core studies, Treat. Geochem., 4, 213–243, doi:10.1016/B0-08-043751-6/04040-8, 2003. 30523

ACPD
13, 30521–30574, 2013

Jouzel, J., Stiévenard, M., Johnsen, S., Landais, A., Masson-Delmotte, V., Sveinbjornsdottir, A., Vimeux, F., von Grafenstein, U., and White, J.: The GRIP deuterium-excess record, Quaternary Sci. Rev., 26, 1–17, doi:10.1016/j.quascirev.2006.07.015, 2007. 30524

Kindler, P., Guillevic, M., Baumgartner, M., Schwander, J., Landais, A., and Leuenberger, M.: NGRIP temperature reconstruction from 10 to 120 kyr b2k, Clim. Past Discuss., 9, 4099–4143, doi:10.5194/cpd-9-4099-2013, 2013. 30541

Krinner, G. and Werner, M.: Impact of precipitation seasonality changes on isotopic signals in polar ice cores: a multi-model analysis, Earth Planet. Sc. Lett., 216, 525–538, doi:10.1016/S0012-821X(03)00550-8, 2003. 30524

Krinner, G., Genthon, C., and Jouzel, J.: GCM analysis of local influences on ice core delta signals, Geophys. Res. Lett., 24, 2825–2828, doi:10.1029/97GL52891, 1997. 30524

Kurita, N.: Origin of Arctic water vapor during the ice-growth season, Geophys. Res. Lett., 38, L02709, doi:10.1029/2010GL046064, 2011. 30525, 30539

Lee, X., Smith, R., and Williams, J.: Water vapour $^{18}O/^{16}O$ isotope ratio in surface air in New England, USA, Tellus B, 58, 293–304, doi:10.1111/j.1600-0889.2006.00191.x, 2006. 30541

Liu, Y., Key, J. R., Ackerman, S. A., Mace, G. G., and Zhang, Q.: Arctic cloud macrophysical characteristics from CloudSat and CALIPSO, Remote Sens. Environ., 124, 159–173, doi:10.1016/j.rse.2012.05.006, 2012. 30540

Majoube, M.: Fractionnement en oxygène 18 et en deutérium entre l'eau et sa vapeur, J. Chim. Phys., 68, 1423–1436, 1971a. 30529

Majoube, M.: Fractionnement en oxygène 18 entre la glace et la vapeur d'eau, J. Chem. Phys., 68, 625–636, 1971b. 30529

Masson-Delmotte, V., Jouzel, J., Landais, A., Stievenard, M., Johnsen, S. J., White, J. W. C., Werner, M., Sveinbjornsdottir, A., and Fuhrer, K.: GRIP Deuterium excess reveals rapid and orbital-scale changes in Greenland moisture origin, Science, 309, 118–121, doi:10.1126/science.1108575, 2005. 30524

Masson-Delmotte, V., Braconnot, P., Hoffmann, G., Jouzel, J., Kageyama, M., Landais, A., Lejeune, Q., Risi, C., Sime, L., Sjolte, J., Swingedouw, D., and Vinther, B.: Sensitivity of interglacial Greenland temperature and $\delta^{18}O$: ice core data, orbital and increased CO_2 climate simulations, Clim. Past, 7, 1041–1059, doi:10.5194/cp-7-1041-2011, 2011. 30524, 30541

Merlivat, L. and Jouzel, J.: Global climatic interpretation of the deuterium-oxygen 18 relationship for precipitation, J. Geophys. Res.-Oceans, 84, 5029–5033, doi:10.1029/JC084iC08p05029, 1979. 30524, 30545

ACPD
13, 30521–30574, 2013

Merlivat, L. and Nief, G.: Fractionnement isotopique lors des changements d'état solide-vapeur et liquide-vapeur de l'eau à des températures inférieures à 0 °C, Tellus, 19, 122–127, doi:10.1111/j.2153-3490.1967.tb01465.x, 1967. 30529

Neff, W., Compo, G., Martin Ralph, F., and Shupe, M.: Continental heat anomalies and the extreme melting of the Greenland ice surface in 2012 and 1889, J. Geophys. Res.-Atmos., submitted, 2013. 30526, 30538

Nghiem, S. V., Hall, D. K., Mote, T. L., Tedesco, M., Albert, M. R., Keegan, K., Shuman, C. A., DiGirolamo, N. E., and Neumann, G.: The extreme melt across the Greenland ice sheet in 2012, Geophys. Res. Lett., 39, L20502, doi:10.1029/2012GL053611, 2012. 30526, 30538

Ortega, P., Swingedouw, D., Masson-Delmotte, V., Risi, C., Vinther, B., Vautard, R., and Yoshimura, K.: Characterizing atmospheric circulation signals in Greenland ice cores: insights from the weather regime approach, Clim. Dynam., submitted, 2013. 30535

Persson, A., Langen, P. L., Ditlevsen, P., and Vinther, B. M.: The influence of precipitation weighting on interannual variability of stable water isotopes in Greenland, J. Geophys. Res.-Atmos., 116, D20120, doi:10.1029/2010JD015517, 2011. 30524

Pfahl, S. and Sodemann, H.: What controls deuterium excess in global precipitation?, Clim. Past Discuss., 9, 4745–4770, doi:10.5194/cpd-9-4745-2013, 2013. 30545

Risi, C., Bony, S., Vimeux, F., and Jouzel, J.: Water-stable isotopes in the LMDZ4 general circulation model: model evaluation for present-day and past climates and applications to climatic interpretations of tropical isotopic records, J. Geophys. Res.-Atmos., 115, D12118, doi:10.1029/2009JD013255, 2010a. 30526, 30535, 30543

Risi, C., Landais, A., Bony, S., Jouzel, J., Masson-Delmotte, V., and Vimeux, F.: Understanding the o-17 excess glacial-interglacial variations in Vostok precipitation, J. Geophys. Res.-Atmos., 115, D10112, doi:10.1029/2008JD011535, 2010b. 30548

Rousseau, D.-D., Duzer, D., Cambon, G., Jolly, D., Poulsen, U., Ferrier, J., Schevin, P., and Gros, R.: Long distance transport of pollen to Greenland, Geophys. Res. Lett., 30, 1765, doi:10.1029/2003GL017539, 2003. 30539

Rozanski, K., Araguás-Araguás, L., and Gonfiantini, R.: Isotopic patterns in modern global precipitation, in: Geophraphical Monograph Series, edited by: Swart, P. K., Lohmann, K. C., McKenzie, J., and Savin, S., vol. 78, American Geophysical Union, Washington DC, 1–36, 1993. 30525

ACPD
13, 30521–30574, 2013

Severinghaus, J. P. and Brook, E. J.: Abrupt climate change at the end of the Last Glacial Period inferred from trapped air in polar ice, Science, 286, 930–934, 10542141, doi:10.1126/science.286.5441.930, 1999. 30524

Sime, L. C., Risi, C., Tindall, J. C., Sjolte, J., Wolff, E. W., Masson-Delmotte, V., and Capron, E.: Warm climate isotopic simulations: what do we learn about interglacial signals in Greenland ice cores?, Quaternary Sci. Rev., 67, 59–80, doi:10.1016/j.quascirev.2013.01.009, 2013. 30541

Sjolte, J., Hoffmann, G., Johnsen, S. J., Vinther, B. M., Masson-Delmotte, V., and Sturm, C.: Modeling the water isotopes in Greenland precipitation 1959–2001 with the meso-scale model REMO-iso, J. Geophys. Res.-Atmos., 116, D18105, doi:10.1029/2010JD015287, 2011. 30524, 30525, 30541, 30546

Sodemann, H. and Stohl, A.: Asymmetries in the moisture origin of Antarctic precipitation, Geophys. Res. Lett., 36, L22803, doi:10.1029/2009GL040242, 2009. 30534

Sodemann, H., Schwierz, C., and Wernli, H.: Interannual variability of Greenland winter precipitation sources: Lagrangian moisture diagnostic and North Atlantic Oscillation influence, J. Geophys. Res.-Atmos., 113, D12111, doi:10.1029/2007JD008503, 2008a. 30524

Sodemann, H., Masson-Delmotte, V., Schwierz, C., Vinther, B. M., and Wernli, H.: Interannual variability of Greenland winter precipitation sources: 2. Effects of North Atlantic Oscillation variability on stable isotopes in precipitation, J. Geophys. Res., 113, D03107, doi:10.1029/2007JD009416, 2008b. 30524, 30526, 30534

Steen-Larsen, H. C., Masson-Delmotte, V., Sjolte, J., Johnsen, S. J., Vinther, B. M., Bréon, F.-M., Clausen, H. B., Dahl-Jensen, D., Falourd, S., Fettweis, X., Gallée, H., Jouzel, J., Kageyama, M., Lerche, H., Minster, B., Picard, G., Punge, H. J., Risi, C., Salas, D., Schwander, J., Steffen, K., Sveinbjörnsdóttir, A. E., Svensson, A., and White, J.: Understanding the climatic signal in the water stable isotope records from the NEEM shallow firn/ice cores in northwest Greenland, J. Geophys. Res.-Atmos., 116, D06108, doi:10.1029/2010JD014311, 2011. 30524, 30525, 30535

Steen-Larsen, H. C., Johnsen, S. J., Masson-Delmotte, V., Stenni, B., Risi, C., Sodemann, H., Balslev-Clausen, D., Blunier, T., Dahl-Jensen, D., Ellehøj, M. D., Falourd, S., Grindsted, A., Gkinis, V., Jouzel, J., Popp, T., Sheldon, S., Simonsen, S. B., Sjolte, J., Steffensen, J. P., Sperlich, P., Sveinbjörnsdóttir, A. E., Vinther, B. M., and White, J. W. C.: Continuous monitoring of summer surface water vapor isotopic composition above the Greenland Ice Sheet,

ACPD
13, 30521–30574, 2013

Atmos. Chem. Phys., 13, 4815–4828, doi:10.5194/acp-13-4815-2013, 2013a. 30525, 30526, 30530, 30535, 30536, 30543, 30546, 30547

Steen-Larsen, H. C., Masson-Delmotte, V., Hirabayashi, M., Winkler, R., Satow, K., Prié, F., Bayou, N., Brun, E., Cuffey, K. M., Dahl-Jensen, D., Dumont, M., Guillevic, M., Kipfstuhl, J., Landais, A., Popp, T., Risi, C., Steffen, K., Stenni, B., and Sveinbjörnsdottír, A.: What controls the isotopic composition of Greenland surface snow?, Clim. Past Discuss., 9, 6035–6076, doi:10.5194/cpd-9-6035-2013, 2013b. 30525

Steffensen, J. P., Andersen, K. K., Bigler, M., Clausen, H. B., Dahl-Jensen, D., Fischer, H., Goto-Azuma, K., Hansson, M., Johnsen, S. J., Jouzel, J., Masson-Delmotte, V., Popp, T., Rasmussen, S. O., Röthlisberger, R., Ruth, U., Stauffer, B., Siggaard-Andersen, M.-L., Sveinbjörnsdóttir, A. E., Svensson, A., and White, J. W. C.: high-resolution Greenland ice core data show abrupt climate change happens in few years, Science, 321, 680–684, doi:10.1126/science.1157707, PMID: 18566247, 2008. 30524

Stephens, B. B., Keeling, R. F., Heimann, M., Six, K. D., Murnane, R., and Caldeira, K.: Testing global ocean carbon cycle models using measurements of atmospheric O2 and CO_2 concentration, Global Biogeochem. Cy., 12, 213–230, doi:10.1029/97GB03500, 1998. 30527

Stohl, A., Forster, C., Frank, A., Seibert, P., and Wotawa, G.: Technical note: The Lagrangian particle dispersion model FLEXPART version 6.2, Atmos. Chem. Phys., 5, 2461–2474, doi:10.5194/acp-5-2461-2005, 2005. 30534

Thomas, E. R., Wolff, E. W., Mulvaney, R., Johnsen, S. J., Steffensen, J. P., and Arrowsmith, C.: Anatomy of a Dansgaard-Oeschger warming transition: high-resolution analysis of the North Greenland Ice Core Project ice core, J. Geophys. Res.-Atmos., 114, D08102, doi:10.1029/2008JD011215, 2009. 30524

Tremoy, G., Vimeux, F., Cattani, O., Mayaki, S., Souley, I., and Favreau, G.: Measurements of water vapor isotope ratios with wavelength-scanned cavity ring-down spectroscopy technology: new insights and important caveats for deuterium excess measurements in tropical areas in comparison with isotope-ratio mass spectrometry, Rapid Commun. Mass Spectr., 25, 3469–3480, doi:10.1002/rcm.5252, 2011. 30525, 30530, 30534

Vinther, B., Jones, P., Briffa, K., Clausen, H., Andersen, K., Dahl-Jensen, D., and Johnsen, S.: Climatic signals in multiple highly resolved stable isotope records from Greenland, Quaternary Sci. Rev., 29, 522–538, doi:10.1016/j.quascirev.2009.11.002, 2010. 30524, 30541

Welp, L. R., Lee, X., Griffis, T. J., Wen, X.-F., Xiao, W., Li, S., Sun, X., Hu, Z., Martin, M. V., and Huang, J.: A meta-analysis of water vapor deuterium-excess in the midlatitude atmo-

spheric surface layer, Global Biogeochem. Cy., 26, GB3021, doi:10.1029/2011GB004246, 2012. 30536

Werner, M., Langebroek, P. M., Carlsen, T., Herold, M., and Lohmann, G.: Stable water isotopes in the ECHAM5 general circulation model: toward high-resolution isotope modeling on a global scale, J. Geophys. Res.-Atmos., 116, D15109, doi:10.1029/2011JD015681, 2011. 30546

ACPD
13, 30521–30574, 2013

Table 1. Theoretical values and humidity correction coefficients for "GREEN" and "EPB" standards, for δD and $\delta^{18}O$. *a*, *b* and *c* are the coefficients used in Eq. (2).

Name	GREEN		EPB	
Isotope	δ^{18}O	δD	δ^{18}O	δD
Value (‰)	-32.99 ± 0.05	-256.0 ± 0.5	-6.12 ± 0.05	-43.2 ± 0.5
a	188.3×10^4	159.6×10^5	117.2×10^3	467.2×10^2
b	444.0	−13 948.0	−618.0	−29 562.9
c	−29.1	−234.6	−4.2	−34.7

ACPD
13, 30521–30574, 2013

Table 2. Summary of experimental difficulties and evolutions which occured on the Picarro instrument between 21 September 2011 and 31 May 2013.

Beginning	End	Failure description	Solution applied	Effects
12 Nov 2011	6 Feb 2012	Ambient air sampling head destroyed by wind	Head replaced, inlet line dried	No ambient air measurement
6 Feb 2012	1 Apr 2012	Calibration system water saturation	Calibration system dried	No calibration
Jul 2012	21 Feb 2013	Leaks on one calibration system SDM syringe	Calibrations with one standard alternated every week (9 Nov 2012 to 21 Feb 2013)	Unstable standard measurements
1 Sep 2012	9 Nov 2012	Simultaneous leaks on both SDM syringes	Syringe cleaned	No calibration
29 Mar 2013	12 Apr 2013	Leaks on calibration air drying system	DRIERITE replaced	No calibration

Date	System evolution	Effects
25 Oct 2012	Manual dry air flow regulator replaced by fixed flow restrictor	Calibrations more stable
21 Feb 2013	SDM ceramic syringes replaced by glass syringes	No more leaks on SDM syringes, calibrations more stable

ACPD
13, 30521–30574, 2013

Table 3. Monthly average (Avg), minimal (Min), maximal (Max) and number (N) of hourly data, for $\delta^{18}O_v$ and d_v, temperature (T), humidity mixing ratio (w) at Ivittuut station from Oct to 2011 to May 2013.

Month	$\delta^{18}O_v$ (‰)			d_v (‰)			N	T (°C)				w (mmol mol^{-1})			
yyyy-mm	Avg	Min	Max	Avg	Min	Max		Avg	Min	Max	N	Avg	Min	Max	N
2011-10	−25.1	−34.0	−17.6	18.4	6.2	38.3	682	0.2	−6.0	9.2	720	4.6	1.5	8.6	682
2011-11	−28.1	−33.4	−22.3	24.9	14.6	43.6	249	−5.7	−11.2	−0.2	264	2.5	1.4	4.9	249
2012-04	−21.9	−30.4	−15.9	11.4	−3.6	28.0	542	1.5	−8.0	12.0	297	6.4	2.7	13.0	604
2012-05	−19.8	−31.2	−14.5	6.9	−3.9	17.2	417	5.3	−0.1	14.2	232	7.6	3.4	11.7	608
2012-06	−17.8	−29.4	−14.9	4.7	−3.9	15.1	602	9.7	6.6	14.7	34	9.5	5.2	12.0	647
2012-07	−19.7	−28.0	−13.6	10.3	1.6	19.3	665	12.4	4.6	21.6	437	11.9	7.6	18.9	676
2012-08	−20.3	−29.1	−14.1	11.2	−1.7	27.1	681	9.5	3.6	17.9	548	10.9	6.6	15.9	687
2012-11	−23.5	−31.8	−16.0	19.9	−0.8	36.4	510	−0.3	−8.5	9.6	600	5.3	2.2	10.7	569
2012-12	−27.1	−36.6	−19.3	15.8	2.0	27.4	468	−2.2	−10.7	10.7	744	4.2	1.5	8.1	567
2013-01	−26.3	−34.5	−18.7	15.4	6.2	33.3	704	−3.6	−14.4	4.4	720	4.0	1.6	8.9	708
2013-02	−24.6	−30.3	−16.3	16.6	7.0	33.1	627	−4.3	−12.8	4.8	672	4.2	1.4	8.4	627
2013-03	−24.0	−34.2	−17.2	15.2	2.8	37.7	605	−0.7	−9.5	9.7	672	4.2	1.6	8.2	605
2013-04	−21.9	−29.7	−14.9	14.6	−4.1	29.6	396	−0.4	−8.4	7.5	408	4.6	1.8	7.9	396
2013-05	−20.9	−27.8	−16.0	11.0	−3.0	33.7	592	2.6	−4.8	12.9	624	6.3	2.7	8.6	592

ACPD
13, 30521–30574, 2013

Table 4. Values of slopes, correlation coefficients (R) and number of data points (N) for relationships between (downwards): $\delta^{18}O_v$ and temperature, $\delta^{18}O_v$ and the logarithm of humidity mixing ratio, d_v and temperature, d_v and $\delta^{18}O_v$, d_v and relative humidity. These values are computed for different timescales using different average data frequencies (from left to right): for the observed diurnal cycle (from 21 to 23 Aug 2012 data) based on hourly data, for the composite synoptic event based on hourly data, for the four seasons based on daily detrended data (anomalies from 15 days running average data) from 21 Sep 2011 to May 2013, for the complete observation period from 21 Sep 2011 to May 2013 based on daily data, and for daily LMDZiso outputs at Ivittuut terrestrial grid cell from 21 Sep 2011 to May 2013.

		Observations							LMDZiso
		Diurnal cycle (hourly)	Composite event (hourly)	Detrented signal on one season (daily)				Complete period (daily)	Complete period (daily)
				Spring	Summer	Autumn	Winter		
$\delta^{18}O/T$	Slope	−0.01	0.76	0.25	−0.20	0.73	0.03	0.37	0.28
	R	−0.06	0.91	0.35	−0.16	0.63	0.04	0.65	0.48
	N	64	97	89	50	67	76	282	467
$\delta^{18}O/\ln(w)$	Slope	2.3	6.2	6.0	9.0	5.5	5.2	5.9	4.4
	R	0.18	0.95	0.69	0.46	0.78	0.59	0.82	0.7
	N	64	97	117	88	70	76	351	467
d_v/T	Slope	0.19	−1.46	−1.15	0.55	−2.11	−0.64	−0.63	−0.056
	R	0.43	−0.84	−0.64	0.32	−0.76	−0.57	−0.62	−0.13
	N	64	97	89	50	67	76	282	467
$d_v/\delta^{18}O$	Slope	−1.60	−1.87	−1.76	−0.92	−1.85	−0.34	−1.40	−0.55
	R	−0.65	−0.90	−0.73	−0.65	−0.77	−0.20	−0.75	−0.72
	N	64	97	117	88	70	76	351	467
d_v/RH	Slope	−0.04	−0.30	−0.20	−0.18	−0.29	−0.09	−0.23	−0.10
	R	−0.37	−0.95	−0.56	−0.64	−0.85	−0.32	−0.63	−0.55
	N	64	97	89	50	67	76	282	467

ACPD
13, 30521–30574, 2013

Table 5. Correlation coefficients R between the different data sets of relative humidity (RH) and d_v from observations, LMDZiso outputs at Ivittuut and in Zone 1. Note that Zone 1 relative humidity from LMDZiso is normalized to SST.

		IVI				Zone 1	
		d_v obs	RH obs	d_v LMDZiso	RH LMDZiso	d_v LMDZiso	RH_{SST} LMDZiso
IVI	d_v obs	–	−0.75	0.37	−0.38	0.71	−0.76
	RH obs	–	–	−0.15	0.20	−0.53	0.69
	d_v LMDZiso	–	–	–	−0.55	0.39	−0.28
	RH LMDZiso	–	–	–	–	−0.11	0.20
Zone 1	d_v LMDZiso	–	–	–	–	–	−0.84
	RH LMDZiso	–	–	–	–	–	–

ACPD
13, 30521–30574, 2013

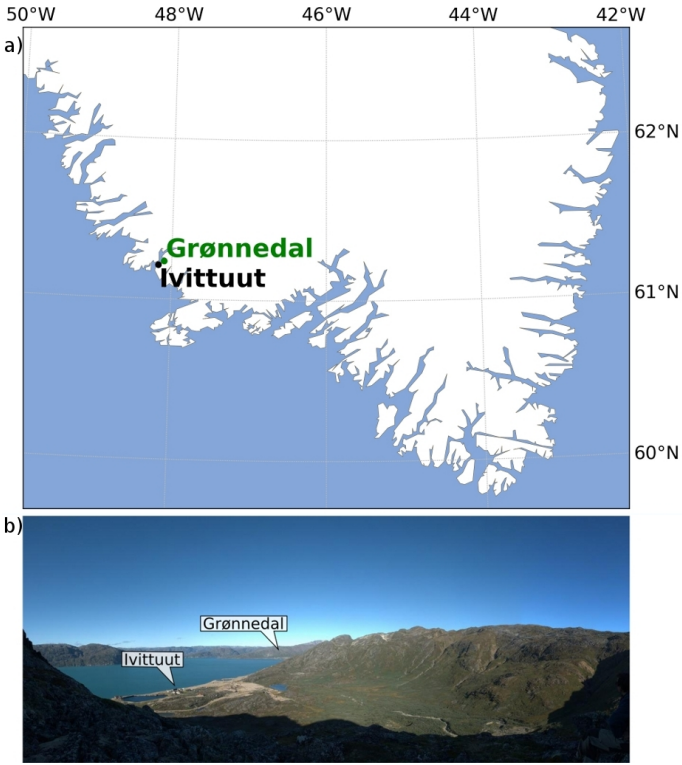

Fig. 1. Southern Greenland map **(a)**. Arsuk Fjord in autumn 2011, seen from south west, showing Ivittuut and Grønnedal **(b)**.

ACPD
13, 30521–30574, 2013

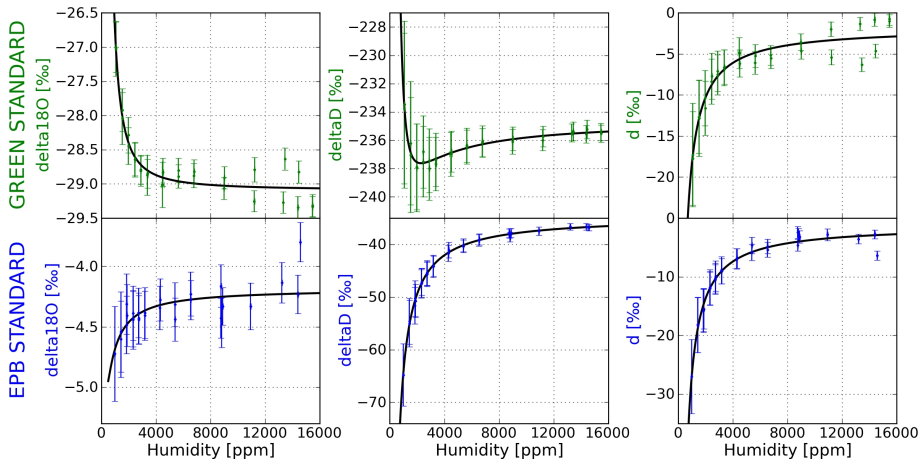

Fig. 2. PICARRO measurements of two reference waters (GREEN and EBP standards) as a function of the humidity mixing ratio, controlled through injection flow of liquid water. The different response functions for δ^{18}O and δD at low humidity levels (below 2000 ppmv) are likely an artifact of residual humidity in the dry air (dried by DRIERITE).

ACPD
13, 30521–30574, 2013

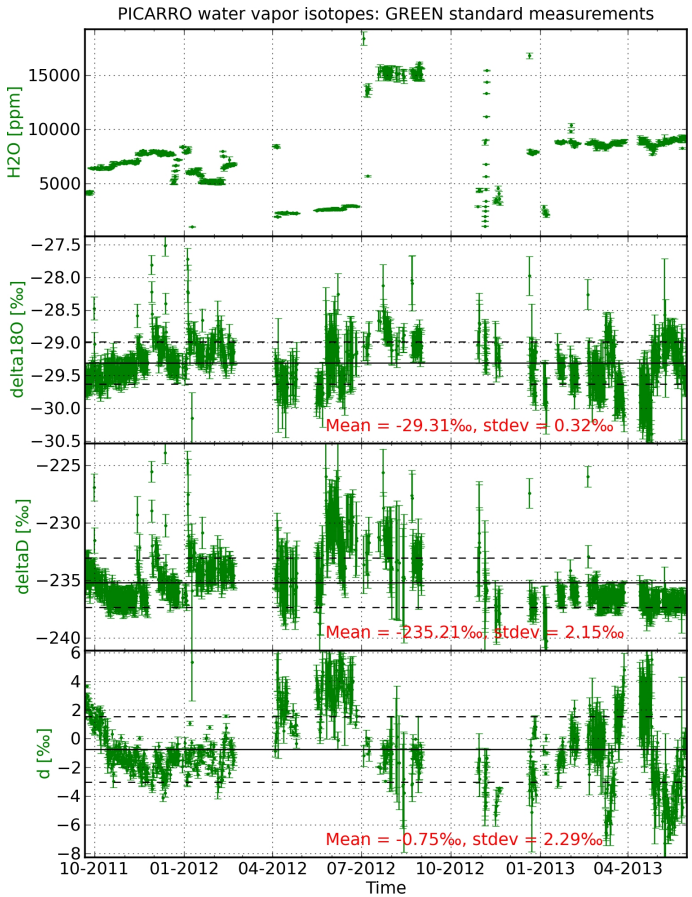

Fig. 3. Successive measurements of GREEN standard for PICARRO calibration: averaged values on the last 20 min of each measurement sequence. Isotopic values are all corrected by Eq. (2) at an arbitrary humidity mixing ratio of 10 000 ppmv. Top to bottom: humidity mixing ratio (ppmv), δ^{18}O (‰), δD (‰) and d (‰).

ACPD
13, 30521–30574, 2013

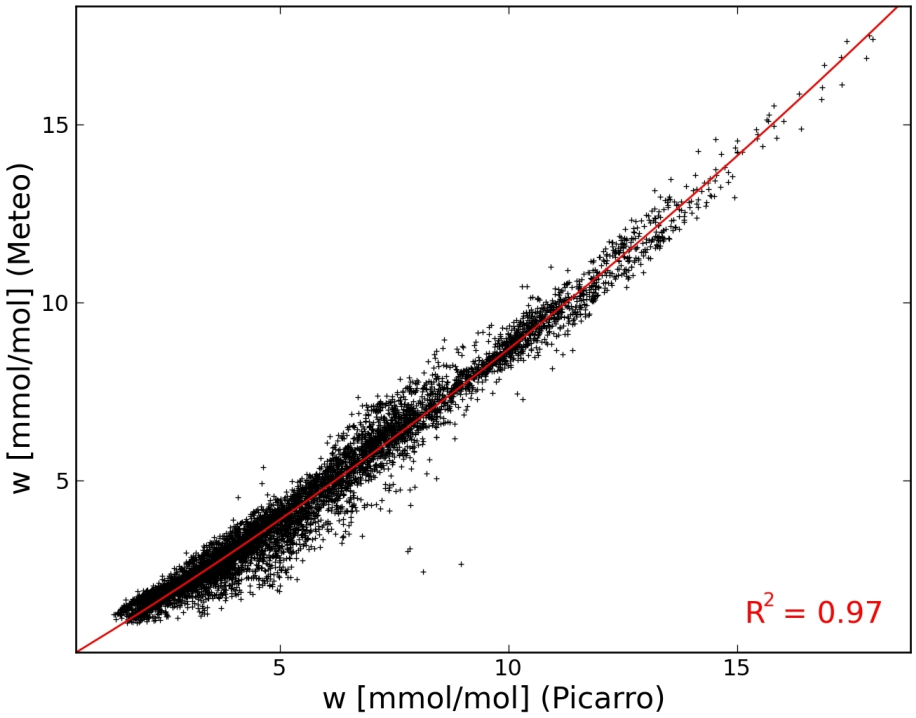

Fig. 4. Black crosses: hourly averaged observations at Ivittuut station from 21 September 2011 to 31 May 2013, Picarro vs. meteorological sensor mixing ratio ($mmol_{water}/mol_{dry\ air}$). Red curve: second order polynomial regression (Eq. 4).

ACPD
13, 30521–30574, 2013

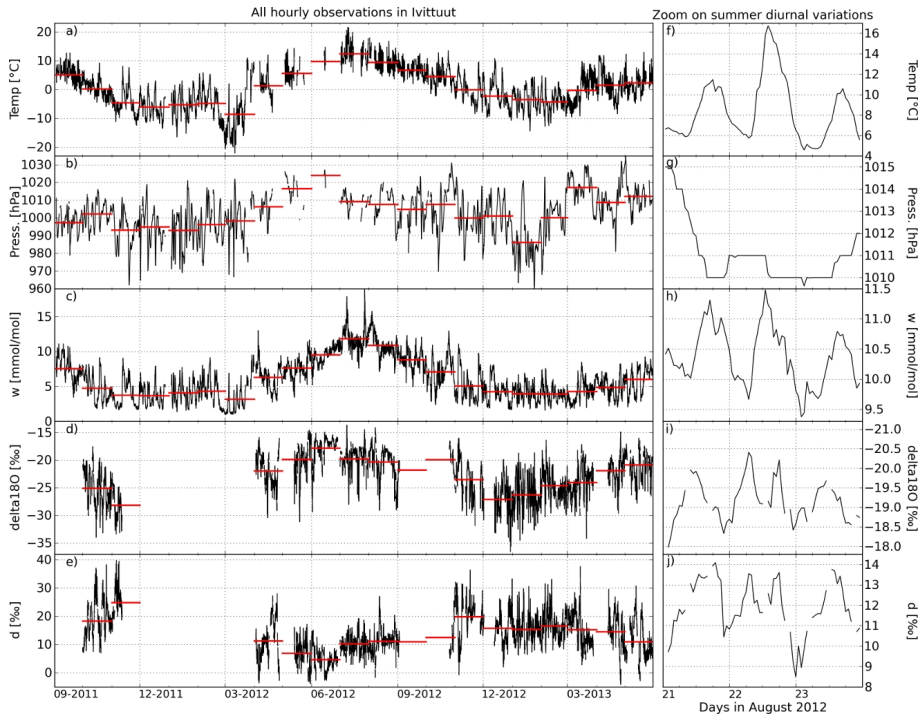

Fig. 5. Hourly observations time-series in Ivittuut from the Picarro instrument and meteorological measurements (black). Monthly averages are shown as red bars. Left column: data from 21 September 2011 to 31 May 2013. Right column: data from 21 to 23 August 2013. Time is in UTC. Top to bottom: temperature (°C) **(a, f)**, pressure (hPa) **(b, g)**, humidity mixing ratio averaged from Picarro and meteorological sensor corrected values ($mmol_{water}/mol_{dry\ air}$) **(c, h)**, $\delta^{18}O$ (‰) **(d, i)** and d (‰) **(e, j)**. Note that the right and left graphs have different vertical scales.

ACPD
13, 30521–30574, 2013

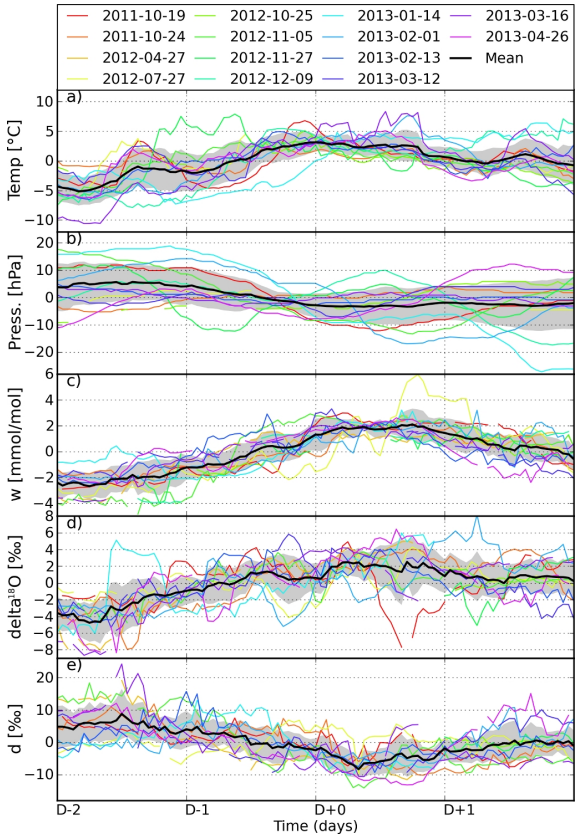

Fig. 6. 4 days time series of 14 synoptic events (color curves) observed at Ivittuut station and composite event mean value (thick black curve) and standard deviation (grey shade). Anomalies are calculated as the difference between hourly values and the averaged values over the 4 days surrounding the humidity increase. Top to bottom: temperature (°C), pressure (hPa), humidity ($mmol_{water}/mol_{dry\ air}$), $\delta^{18}O$ (‰) and d (‰).

ACPD
13, 30521–30574, 2013

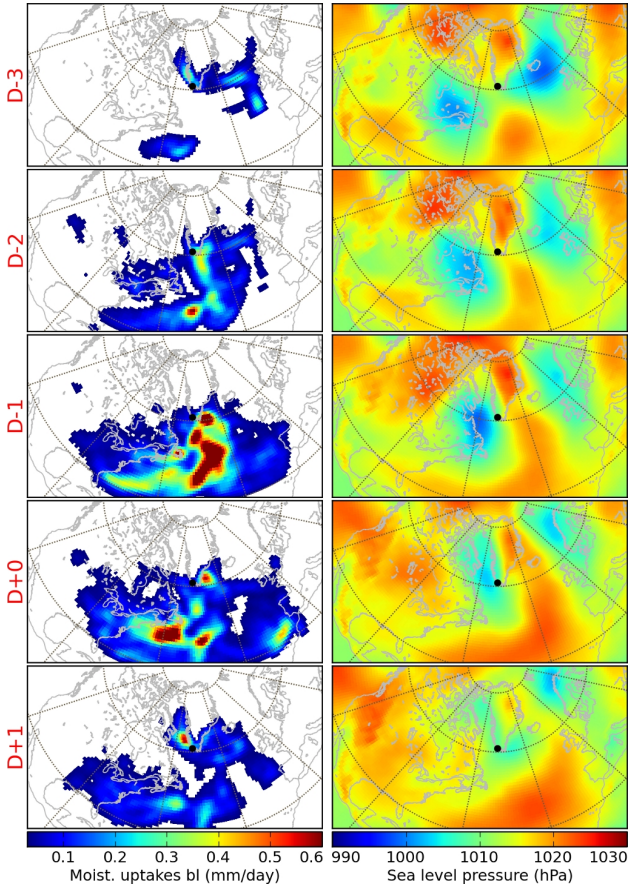

Fig. 7. Moisture uptake sources in mm/day for air masses arriving in Ivittuut (left) and sea level pressure from ECMWF ERA-Interim reanalyses (right) during 5 days surrounding 14 synoptic events on the period 21 September 2011 to 31 December 2012.

ACPD
13, 30521–30574, 2013

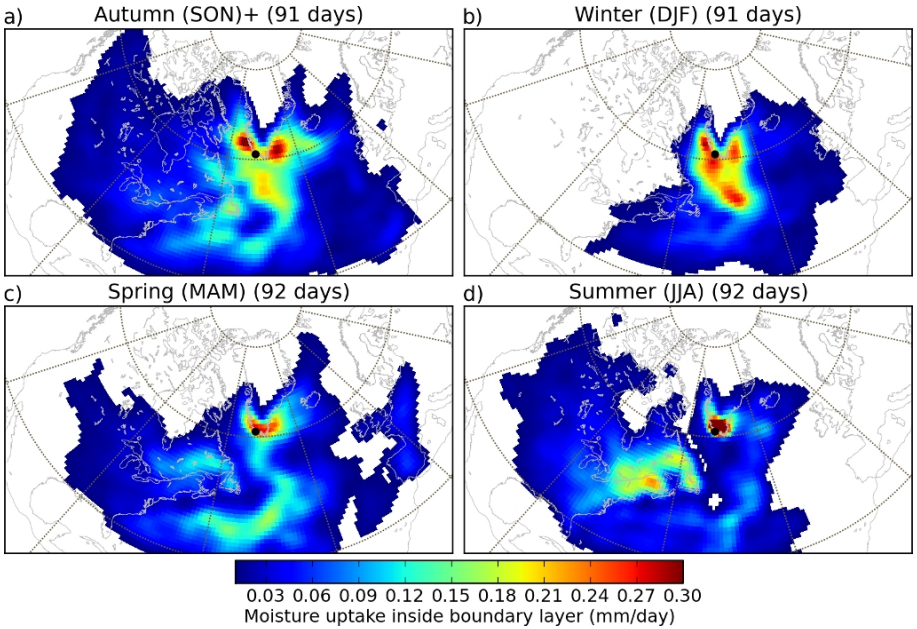

Fig. 8. Moisture uptake sources (in mm day^{-1}) for air masses arriving in Ivittuut, averaged by season for year 2012.

ACPD
13, 30521–30574, 2013

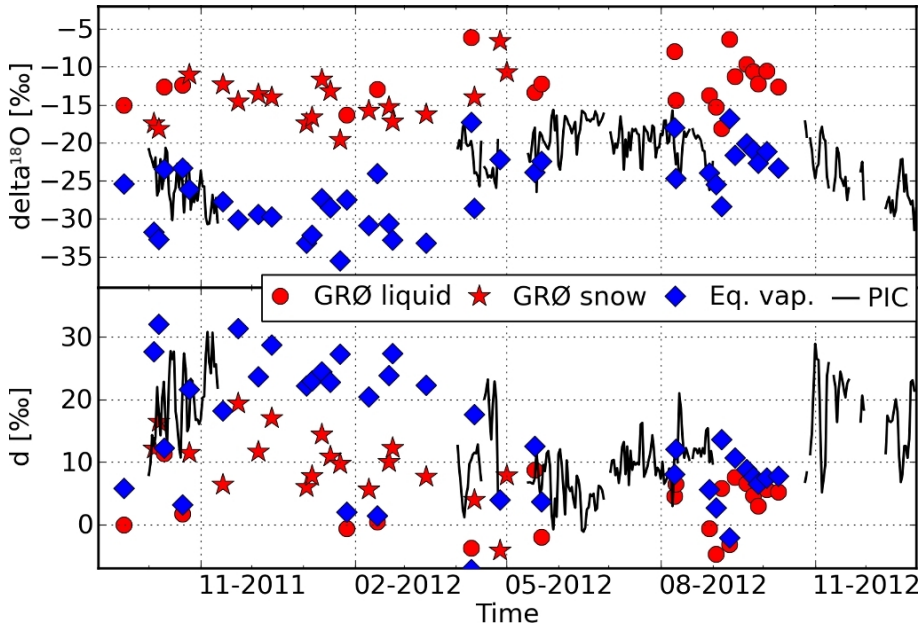

Fig. 9. Top to bottom: δ^{18}O (‰) and d (‰). Black curves represent water vapour observations daily averaged values (δ_v and d_v); red circles and stars represent precipitation samplings isotopic composition liquid and snow samples respectively (δ_p and d_p); blue diamonds represent water vapour isotopic composition calculated from precipitation measurements supposing phase change at equilibrium ($\delta_{v,\,eq}$ and $d_{v,\,eq}$).

ACPD
13, 30521–30574, 2013

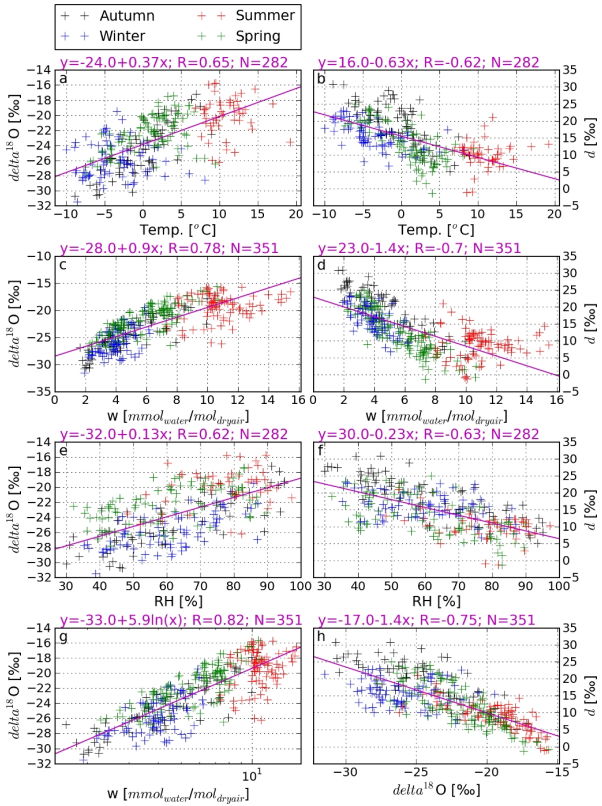

Fig. 10. Crosses: daily averaged observations at Ivittuut station from 2011 September 21 to 2013 May 31 for spring (green), summer (red), autumn (black) and winter (blue). Magenta: linear regression curves (or log-linear regression for **(g)**). $\delta^{18}O_v$ (‰) vs temperature (°C) **(a)**, d_v (‰) vs temperature (°C) **(b)**, $\delta^{18}O_v$ (‰) vs w ($mmol_{water}/mol_{dry\ air}$) **(c)**, d_v (‰) vs w ($mmol_{water}/mol_{dry\ air}$) **(d)**, $\delta^{18}O_v$ (‰) vs RH (%) **(e)**, d_v (‰) vs RH (%) **(f)**, $\delta^{18}O_v$ (‰) vs w ($mmol_{water}/mol_{dry\ air}$) in log scale **(g)**, $\delta^{18}O_v$ (‰) vs d_v (‰) **(h)**, **(i)**.

ACPD
13, 30521–30574, 2013

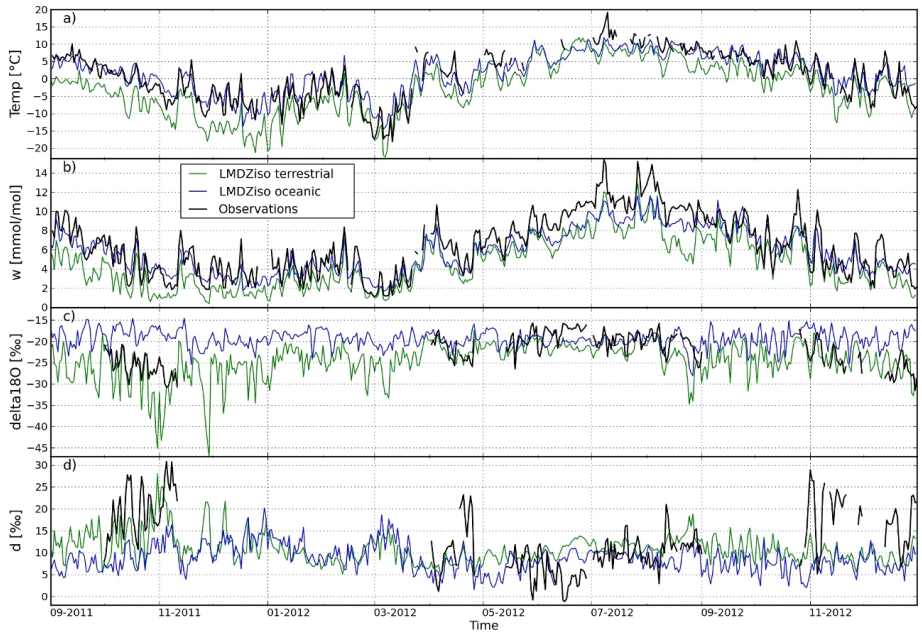

Fig. 11. Time series (from 1 September 2011 to 31 December 2012) of LMDZiso at Ivittuut terrestrial grid cell (62.11° N, 48.75° W) (green curves), LMDZiso at the nearest oceanic grid cell (62.11° N, 52.5° W (blue curves) and observations in Ivittuut (black curves). Temperature (°C) **(a)**, humidity mixing ratio ($mmol_{water}/mol_{dry\ air}$) **(b)**, $\delta^{18}O$ (‰) **(c)** and d (‰) **(d)**. Observed humidity mixing ratio in computed as the averaged from Picarro and meteorological sensor derived measurements.

ACPD
13, 30521–30574, 2013

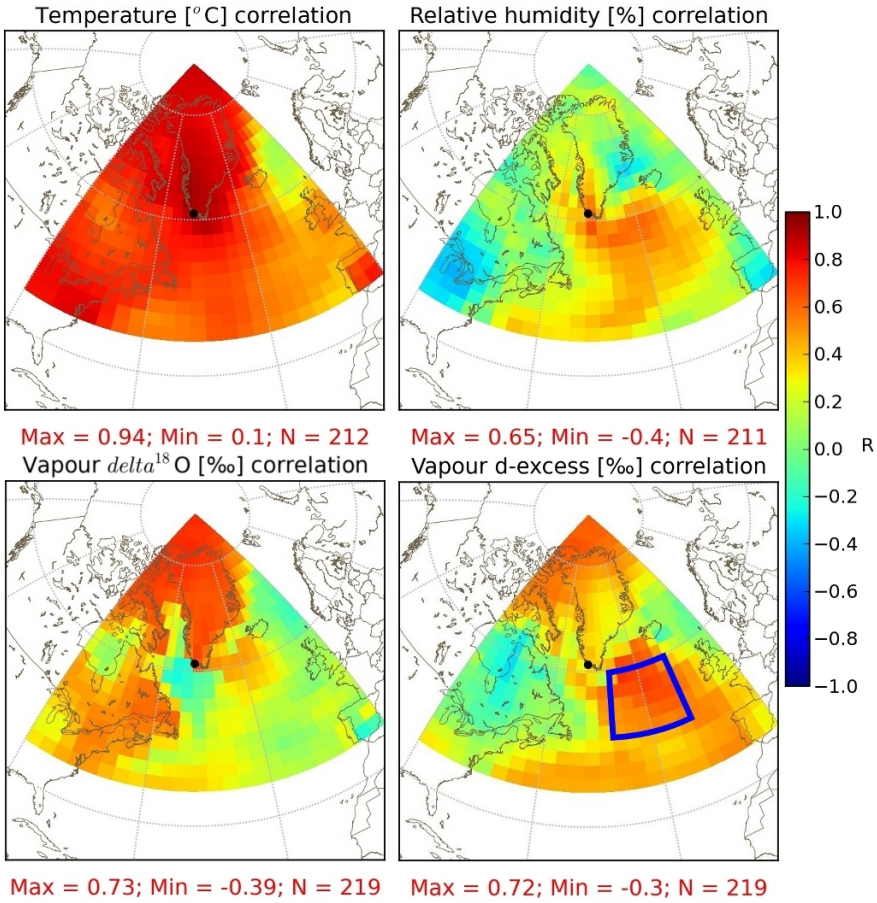

Fig. 12. Maps of correlations between Ivittuut daily observations and LMDZiso simulated daily values at different grid cells, for temperature, relative humidity, $\delta^{18}O_v$ and d_v. Color indicates R correlation coefficient. Blue square on lower right box represents the region called "Zone 1".

ACPD
13, 30521–30574, 2013

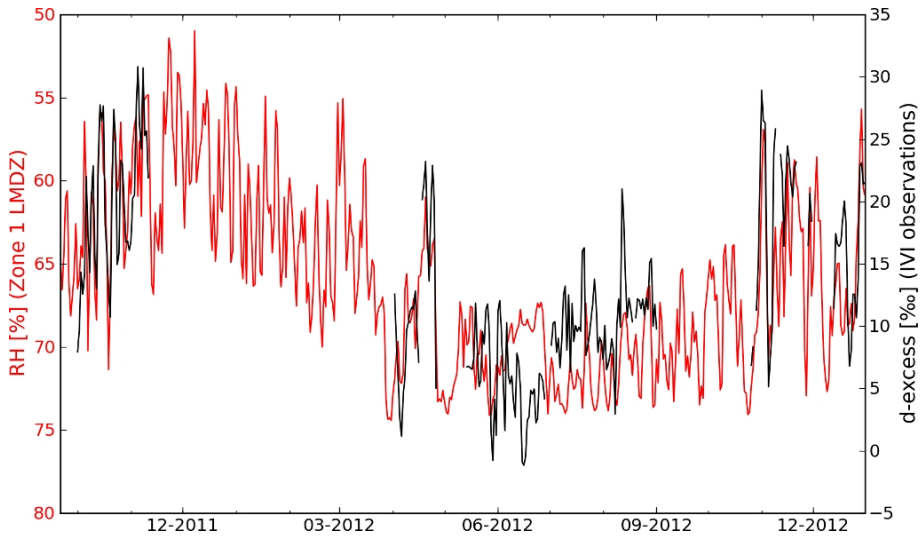

Fig. 13. Red: relative humidity (normalized to SST) (%) averaged over Atlantic region from 49.4366° N, 41.25° W to 59.5775° N, 22.5° W, extracted from LMDZiso simulations, from September 2011 to December 2012. Black: d_v (‰) observed at Ivittuut station on the same period. Note that LMDZiso relative humidity is very similar to that from ECMWF analyses.

ACPD
13, 30521–30574, 2013